Received: 21 August 2022 | Revised: 20 January 2023 | Accepted: 25 January 2023

DOI: 10.1111/bre.12756

Basin Research | IAS EAGE | WILEY

RESEARCH ARTICLE

Structural analysis and measured extension in fault complexes along the Lofoten-Vesterålen margin, offshore Norway, in the context of crustal-scale rifting towards breakup in NE Atlantic

Juan Camilo Meza-Cala[1,2] | **Filippos Tsikalas**[1,3,4] | **Mansour M. Abdelmalak**[1,2] | **Jan Inge Faleide**[1,2]

[1]Department of Geosciences, University of Oslo, Oslo, Norway

[2]Centre for Earth Evolution and Dynamics (CEED), University of Oslo, Oslo, Norway

[3]Vår Energi ASA, Stavanger, Norway

[4]Eni E&P, STEX, Milan, Italy

Correspondence
Juan Camilo Meza-Cala, Department of Geosciences, University of Oslo, P.O. Box 1028 Blindern, Oslo NO-0316, Norway.
Email: juancme@geo.uio.no

Abstract

Late Cretaceous–Palaeocene continental extension within the Lofoten-Vesterålen margin is investigated by integrating 2D-3D seismic and potential field datasets, together with updated crustal transects. Most of that deformation is recorded by two low-angle detachment structures named West Røst High Fault Complex (WRHFC) and North Utrøst Ridge Fault Complex (NURFC) located at the southern and central-northern portions of the studied area, respectively. Multiple extensional episodes of various intensities were mapped as different fault stages, including one Albian-Cenomanian phase, four early Late Cretaceous phases, three Late Cretaceous to latest Cretaceous–Palaeocene phases, and one Palaeocene phase. The WRHFC is narrower in extent and has accommodated a relatively greater amount of localized extension (ca. 18–19 km), whereas the NURFC occupies a wider area with widespread extension intensity (ca. 6–8 km). In comparison, the total across-margin average extension within the southern, central, and northern portions of the Lofoten-Vesterålen and NE Greenland conjugate margins are ca. 192, 221, and 266 km, respectively. Such results indicate an apparent extension discrepancy between derived extension from measured fault-block geometries within the fault complexes and the whole conjugate margin system, with only ca. 11% and 13% of the extension seen on the studied seismic profiles on the WRHFC and NURFC, respectively. The corrected maximum extension for purely sub-seismic resolution faulting on both the WRHFC and NURFC fault complexes is ca. 164 and 46 km, respectively. Finally, both WRHFC and NURFC structures provide key evidence for a ductile mode of deformation towards breakup that is expressed through shear zones-rift topography interactions with overlaying listric/detachment faults. These features reflect the resulting multiphase tectonic evolution across the asymmetric Lofoten-Vesterålen and NE Greenland conjugate margins, and the obliquity in the

breakup axis location along them. The study outcomes are pertinent and applicable to understand the breakup evolution of the northern NE Atlantic and its vicinity.

KEYWORDS

continental crust extension, Lofoten-Vesterålen margin, low-angle detachment structures, multiphase faulting, NE Atlantic, sub-seismic resolution faulting

1 | INTRODUCTION

Quantifying extension as a function of depth at rifted margins needs to include upper crust fault analysis and estimates of the amount of deformation within sedimentary basins in order to avoid under-prediction of the measured extension (e.g., Kusznir et al., 2005; McDermott & Reston, 2015; Reston, 2007; Reston & McDermott, 2014; Skogseid et al., 1992). Furthermore, rifted margins are often characterized by the so-called extension discrepancy, which refers to the amount of extension measurable from seismically-observed brittle faulting that is far less than that required to explain the observed crustal stretching or thinning. This discrepancy may be due to a combination of several factors including crustal depth-dependent thinning (Davis & Kusznir, 2004), the minor slip produced by relatively smaller faults that can be imaged or detected with seismic reflection methods (Marrett & Allmendinger, 1992; Walsh et al., 1991), the unrecognized polyphase and top basement faulting (Reston, 2005, 2009), and the overlooked sequential faulting that cuts the hanging wall of previously-formed faults (Ranero & Pérez-Gussinyé, 2010). Detailed case studies on well-imaged rifted margins are therefore very valuable as they will highlight important observations related to the imposed structuration and will provide additional constraints and parameters for the proper analysis and quantification of extensional deformation.

The continental margins off Norway and Greenland are conjugate margins that experienced a long history of post-Caledonian extension (since late Devonian at ca. 380 Ma) until breakup at Palaeocene/early Eocene times (Figure 1) (e.g., Abdelmalak et al., 2017; Brekke, 2000; Faleide et al., 2008; Gernigon et al., 2020, 2021; Hamann et al., 2005; Skogseid et al., 2000; Tsikalas, Eldholm, et al., 2005; Zastrozhnov et al., 2018, 2020). Within this context, however, information of crustal extension along the largest part of the Lofoten-Vesterålen Margin (LVM) is limited as existing studies have mainly concentrated in the southernmost LVM and the nearby well-studied Vøring margin (e.g., Abdelmalak et al., 2016, 2017; Skogseid, 1994; Skogseid et al., 1992, 2000; Tsikalas et al., 2008). The LVM has not been opened for petroleum exploration (Norwegian Petroleum Directorate, 2010, 2020a), and thus is one of the least understood rifted margins of the Norwegian continental shelf. Nevertheless, recently updated mapping on the southern and northern segments of the LVM has identified two prominent Late Cretaceous–Palaeocene low-angle detachment fault complexes informally named the West Røst High Fault Complex (WRHFC) and the North Utrøst Ridge Fault Complex (NURFC), respectively (Meza-Cala et al., 2021; Tsikalas et al., 2019) (Figure 2).

Highlights

- Refined Late Cretaceous–Palaeocene rifting by studying two low-angle detachment fault complexes.
- Four extensional pulses of varying intensities are revealed by nine mapped fault stages.
- Stretching/thinning factors are calculated for the continental extension leading to breakup.
- Sub-seismic resolution faulting is accounted to properly estimate extension in the area.
- Multiphase evolution and ductile deformation towards breakup in the Lofoten-Vesterålen margin.

In this study, we aim to better understand continental crustal extension along the LVM through the thorough study of two low-angle detachment fault complexes. The analysis integrates reprocessed 2D seismic reflection data along with the most recently acquired 2D and 3D datasets, potential field (gravity and magnetic) data, and selected updated published crustal transects for the LVM and NE Greenland conjugate margins. Through seismic interpretation and detailed structural measurements, we aim to estimate along the LVM the amount of brittle extension towards breakup from rift-related faults and fault-block geometries and to derive extension estimates from crustal stretching. Furthermore, we investigate whether sub-seismic faulting exists and may contribute to an underestimation of brittle crustal extension both locally and in a regional conjugate margin context.

2 | GEOLOGICAL SETTING

The Lofoten-Vesterålen Margin (LVM) is a ca. 400-km-long rifted margin located at ca. 67–69°N off mainland Norway

(Figure 1). It represents the link between the mid-Norwegian, SW Barents and conjugate NE Greenland margins, and is a key area to study the tectono-stratigraphic evolution of the NE Atlantic margins (Figure 1) (e.g., Faleide, Bjørlykke, et al., 2015; Faleide, Zastrozhnov, et al., 2022; Gernigon et al., 2020, 2021; Tsikalas et al., 2012, 2022; Zastrozhnov et al., 2018, 2020). Moreover, the LVM has its widest portion just north of the Bivrost Lineament and close to the Vøring margin (ca. 150 km in south Lofoten margin), while it narrows towards the north when approaching the Senja Fracture Zone in the vicinity of the SW Barents Sea (ca. 35 km offshore Andøya) (Figure 1) (e.g., Tasrianto & Escalona, 2015; Tsikalas et al., 2001, 2019, 2022). Observations on rift geometries in the conjugate margins led to the proposal of a rifting model with an upper- and lower-plate margin configuration (e.g., Meza-Cala et al., 2021; Mosar et al., 2002; Voss & Jokat, 2009), which involves subsequent magmatic overprinting, and passive margin evolution (e.g., Barnett-Moore et al., 2018; Eldholm & Coffin, 2000; Eldholm et al., 2002; Faleide et al., 2008; Faleide, Abdelmalak, et al., 2022; Faleide, Wong, et al., 2022; Tsikalas et al., 2002, 2012). Recent studies along parts of the proximal and necking domains of the Lofoten-Vesterålen margin (Tasrianto & Escalona, 2015) suggested that the two Late Cretaceous–Palaeocene WRHFC and NURFC fault complexes record much of the experienced tectonism towards breakup (Figure 1; Meza-Cala et al., 2021; Tsikalas et al., 2019). Similar fault complexes with low-angle detachment character have been also documented on the Vøring margin (e.g., Gernigon et al., 2003, 2004; Ren et al., 1998), SW Barents Sea (e.g., Blaich et al., 2017; Koehl et al., 2018), and NE Greenland margin (e.g., Rowan & Jarvie, 2020; Tsikalas, Faleide, et al., 2005).

2.1 | West Røst High Fault Complex

The WRHFC lies in the southern part of the LVM and west of the Røst High (Figures 1 and 2 profile A). It is characterized by NE–SW trending and W-dipping faults that assemble a geometry of independent and rotated fault-blocks. In general, the faults in the complex have planar geometries in the upper parts and become more listric and low-angle with depth. The easternmost faults in the complex form a detachment/décollement plane that mostly runs subparallel to the underlying Base Cretaceous Unconformity (BCU) and the shale-dominated lowermost Cretaceous strata (Figure 2). Both fault geometry and fault-block rotation are noticed to be influenced by basement topography underneath the fault complex (Figure 3) (Tsikalas et al., 2019). Maximum fault throws are in the order of 1 s twt (two-way traveltime) (ca. 1.4 km) and are observed in the central parts of the fault complex, whereas fault throw displacement and dip increase towards the south and west. Moreover, the Base Tertiary Unconformity (BTU) has been identified with a strong erosional unconformity in the upper parts of the fault complex, indicating more pronounced and inflated geometries of the sedimentary packages (Figure 2). Furthermore, a compressional dome (South Lofoten Margin Dome, SLMD) is in close proximity to the WRHFC (Figures 1 and 2) and has evidenced multiple stages of inflation/deflation of the fault complex in response to the post-Palaeocene tectonic activity in the southern LVM (Tsikalas et al., 2019).

2.2 | North Utrøst Ridge Fault Complex

In the northern part of the LVM, a second fault complex, the NURFC (Figure 2 profile B), with similar characteristics as the WRHFC onsets from offshore the Vesterålen to the Andøya islands, and farther north in the southern vicinity to the Harstad Basin (Figure 1). On both the gravity and magnetic data, the NURFC, unlike the WRHFC, shows strong negative anomalies (Figure 3) and this is in accordance with the large thickness of sediments in the hanging-wall growth sequences within the fault complex (Meza-Cala et al., 2021). The NURFC is broad in width (>36 km) and covers a wide area (ca. 1200 km^2) as it develops towards the northernmost LVM (Figures 1 and 3). These are the most striking differences in comparison to the WRHFC, which is narrower in extent and with deformation mainly localized within a portion in the inner-to-outer margin transition. Both the WRHFC and NURFC mainly involve Upper Cretaceous sequences in their hanging-walls, and sedimentary wedges of Palaeocene strata are often present towards the upper parts of the NURFC. In terms of fault geometries, the NURFC contains similar fault shapes as those of the WRHFC, and the NURFC includes easternmost faults with low-angle detachment character gradually propagating to the west (Figure 2). Similarly, the fault throw intensities in both fault complexes are observed to increase in a seaward direction. In addition, the westernmost and steeper Palaeocene faults impede the eastward up-dip flow of lavas on top of the NURFC, and demonstrate that the fault complex was an elevated feature prior to continental breakup and the extrusion of the lava flows (Figure 2). Furthermore, the NURFC has been linked with the evolution and development of the northern LVM in terms of margin segmentation and basin architecture, as well as post-Palaeocene vertical movements expressed as dome-like features (i.e. Northern Vesterålen margin Dome; NVMD) (Figures 1 and 2) (Meza-Cala et al., 2021).

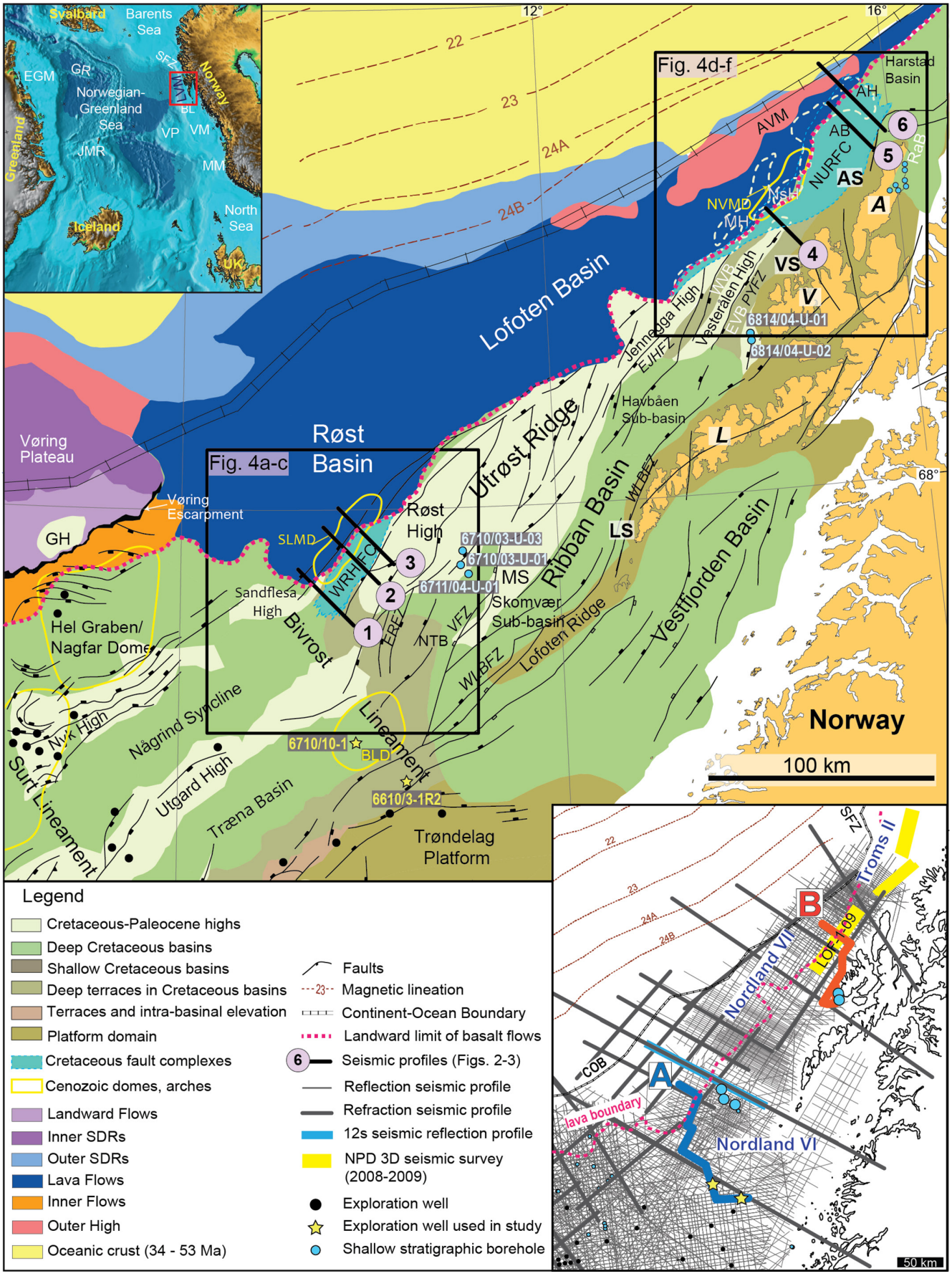

FIGURE 1 Structural map of the Lofoten-Vesterålen margin (LVM) and adjacent margins. Inset (top-left): Norwegian continental margin formed in response to Cenozoic opening of the Norwegian-Greenland Sea as expressed in bathymetry/topography from the 1 × 1′ elevation grid of Jakobsson et al. (2000). Inset (bottom-right): seismic reflection and refraction coverage, and exploration provinces within LVM. The 3D seismic survey LOF-1-09 is indicated in inset, and it was available and utilized in this study. Selected seismic profiles locations (1 to 6; Figures 2 and 3) within the low-angle detachment fault complexes (WRHFC and NURFC), and the focus study portions (zoomed areas) within the black boxes (Figure 4) are also indicated. A, Andøya island; AB, Andøya Basin; AH, Andenes High; AS, Andøya segment; AVM, Andøya Volcanic Mound; BL, Bivrost Lineament; BLD, Bivrost Lineament Dome; EGM, East Greenland margin; EJHFZ, East Jennegga High Fault Zone; ERFZ, East Røst Fault Zone; EVB, East Vesterålen Basin; GH, Grimm High; GR, Greenland Ridge; JMR, Jan Mayen Ridge; L, Lofoten islands; LS, northern Lofoten segment; LVM, Lofoten-Vesterålen margin; MH, Myre High; MM, Møre margin; MS, Marmæle Spur; NsH, Nøss High; NTB, northern Træna Basin; NURFC, North Utrøst Ridge Fault Complex; NVMD, northern Vesterålen margin Dome; PYFZ, Pyramiden Fault Zone; RaB, Ramså Basin; SDRs, seaward-dipping reflections; SFZ, Senja Fracture Zone; SLMD, southern Lofoten margin Dome; V, Vesterålen islands; VFZ, Vesterdjupet Fault Zone; VM, Vøring margin; VP, Vøring Plateau; VS, Vesterålen segment; WLBFZ, West Lofoten Border Fault Zone; WRHFC, West Røst High Fault Complex; WVB, West Vesterålen Basin.

3 | DATA AND METHODS

Reprocessed and recently acquired 2D and 3D seismic reflection datasets in the area by the Norwegian Petroleum Directorate (NPD) were utilized (Figure 1) (for details on utilized seismic datasets see Meza-Cala et al., 2021 and Tsikalas et al., 2019). In order to measure brittle upper crustal extension within the two fault complexes, five 2D multi-channel seismic (MCS) profiles and one 2D-3D composite MCS profile have been selected (six profiles in total); three along the WRHFC in the southern LVM (profiles 1–3) and three along the NURFC in the northern LVM (profiles 4–6) (Figures 4 and 5). The highest seismic resolution (in average good) is found within the southern LVM; i.e. vertical resolution of 34–43 m at 1–2 s twt window. However, below the lava flows to the west the imaging becomes poor; i.e. vertical resolution of 92–98 m at 4–5 s twt window. The recording time of the various MCS surveys ranges between 6–8 s twt. The seismic interpretation of the selected profiles is based upon the recently revised tectono-stratigraphic framework for the different segments of the LVM (Figure 2) (cf. Meza-Cala et al., 2021; Tsikalas et al., 2019, 2022). Gravity and magnetic data (courtesy of Geological Survey of Norway, NGU; e.g., Olesen et al., 2010) for the entire LVM were also available (in this study the focused portions are illustrated), and helped to further support seismic interpretation and structural trends in the vicinity of the fault complexes (Figure 3).

Brittle extension estimates from the selected seismic profiles have been calculated through measurement of fault components, such as heave and displacement, within both the WRHFC and NURFC fault complexes (Figures 4 and 5). The slip vector is assumed parallel to the analysed seismic lines even if we acknowledge that many lines are oblique to some faults systems, and the extension direction may also be oblique (not perpendicular) to some faults. Fault heaves were measured (in kilometres) along the horizontal separation of each seismic horizon or sequence reflection, whereas fault throws were initially estimated in time (s, twt) and then depth-converted using an interval velocity of 2.75 and 2.45 km/s for the Upper Cretaceous and Palaeocene sequences, respectively (velocity information from sonobuoy and ocean-bottom seismometer record sections; see Tsikalas, Eldholm, et al., 2005). Subsequently, fault displacements were calculated (in kilometres) as the longest segment (hypotenuse) of the triangle-rectangle conformed by the fault heave and throw (e.g., Fossen, 2010). No decompaction techniques were implemented to the selected profiles. In addition, stretching factor estimates related to brittle extension (β_f) that are defined by the resulting angles from the fault geometry were calculated on few selected rotated fault-blocks within both the WRHFC and NURFC in order to further investigate considerations on the mode of deformation towards breakup (utilized methodology illustrated in Figures 4 and 5). The stretching factor from fault-block geometries (β_f) was estimated following the Reston (2005) empirical formula: $\beta_f \cong \sin\theta/\sin(\theta-\varphi)$; where θ is the fault-plane inclination, and φ is the top of fault-block angle.

Furthermore, we utilized three pairs of crustal transects (six profiles in total) along the Lofoten-Vesterålen and NE Greenland conjugate margins. The paired conjugate profiles are described as the "southern transect" in the vicinity of the Bivrost Lineament and its conjugate counterpart, the "central transect" across the northern Lofoten segment/Vesterålen-central Danmarkshavn Ridge, and the "northern transect" across the northern Andøya segment-northern Danmarkshavn Ridge (Figure 6). The compiled crustal transects have been revised from Abdelmalak et al. (2022), depict an updated representation of the entire crustal architecture, and are used for measuring total extension across the conjugate margins (see Supporting

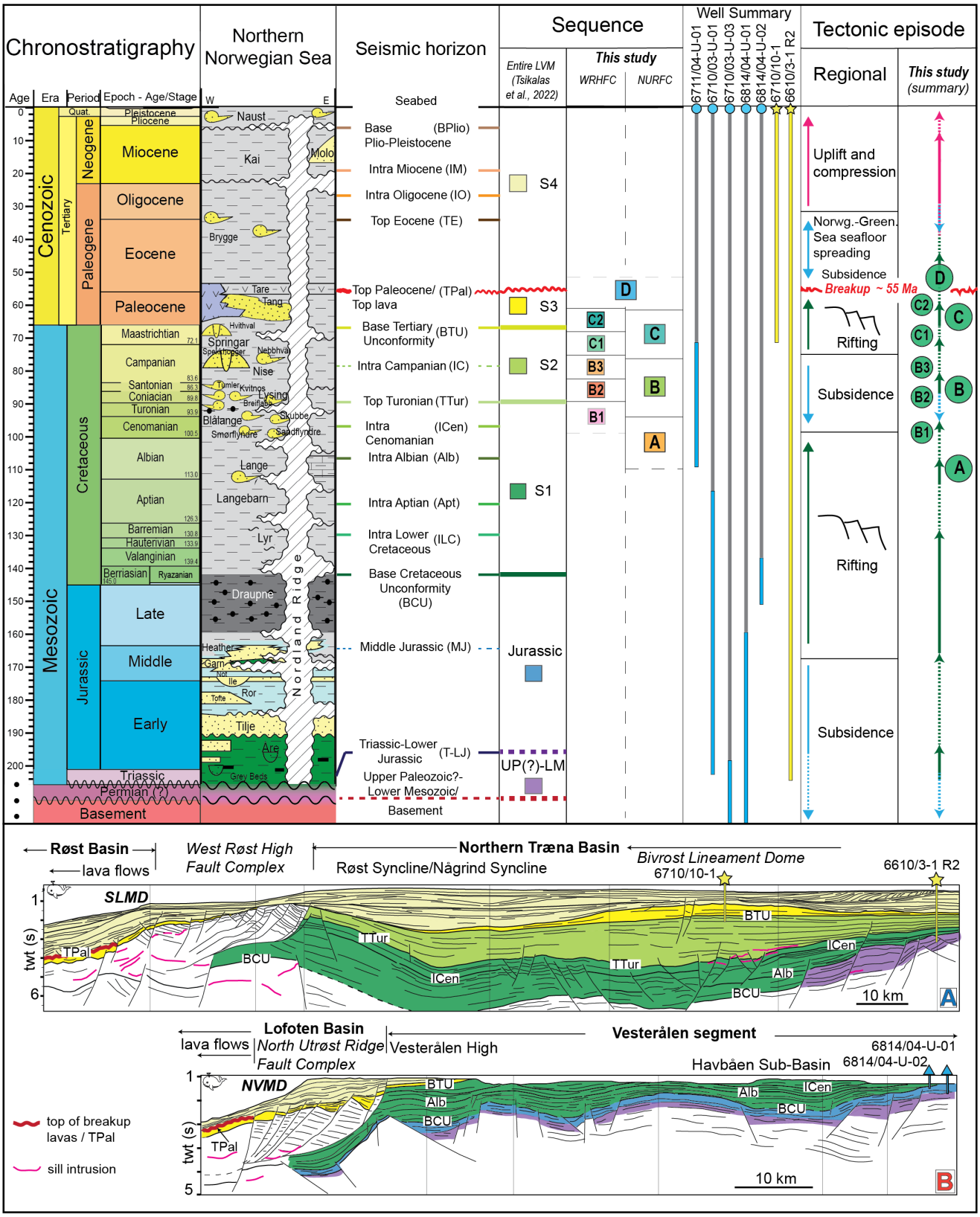

Information). The calculations derive through stretching and thinning factor measurements based on the thickness of the crystalline crust along each transect current (final stretched) length set from the continent-ocean boundary (COB) position and compared to an initial reference crust thickness of 35 km of assumed unstretched continental crust (UCC) (Abdelmalak et al., 2022). The COB was defined as the oceanward limit of the stretched continental

FIGURE 2 Seismic tectono-stratigraphic framework used in this study for the seismic and structural interpretation of the WRHFC and NURFC fault complexes and nearby Lofoten-Vesterålen margin (LVM) vicinity (modified from Tsikalas et al., 2022). Chronostratigraphic and lithostratigraphic charts of the Northern Norwegian Sea modified from Norlex (2012), and geologic time scale after Gradstein et al. (2012). Both exploration and IKU shallow boreholes are indicated in yellow stars and blue circles, respectively (Norwegian Petroleum Directorate, 2020b). Regional tectonic episodes based on Tsikalas et al. (2012). The subdivision of the fault stages within each fault complex interpreted in seismic profiles 1–6 (Figures 4 and 5) is indicated with boxes of different colours and letters. Abbreviations of fault stages at WRHFC (B1–3, C1–2, D) and at NURFC (A, B, C, D) are indicated in Figures 2 and 3. Geoseismic cross-sections (A and B; Tsikalas et al., 2022) are in the bottom and illustrate regional basin stratigraphy and well ties. The transect A and B locations and other abbreviations are in Figure 1.

crust based on the location of seafloor spreading magnetic anomalies in the oceanic crust and the landward limit of undisputed oceanic crust on seismic refraction profiles (Abdelmalak et al., 2022). In addition, the COB corresponds to the transition from oceanic lithosphere to continental lithosphere, and this boundary can form a narrow band or zone of varying width (alternatively the continent-ocean transition; COT) rather than a discrete limit (e.g., Gernigon et al., 2020). Along the NE Atlantic volcanic margins, the COB is frequently masked by magmatic rocks linked to the breakup process (Berndt et al., 2001; Eldholm et al., 2000), significantly complicating its along-margin identification. Moreover, the crystalline crust thickness was estimated up to the mid-Permian level (Abdelmalak et al., 2022). Hence, this stratigraphic level is considered in this study as equivalent to top basement, since it marks the initiation of the multi-rift setting in the NE Atlantic margins following the collapse of the Caledonides (e.g., Faleide et al., 2018). Eclogites are present both onshore Greenland and Norway, which indicate syn-orogenic to probably early post-orogenic crustal thicknesses of ca. 80–90 km (Andersen & Jamtveit, 1990; Brueckner et al., 1998). Our defined top basement in the crustal transects, therefore, does not consider the root of the previous orogenic system, yet it allows a simple calculation of crustal extension since mid-Permian times. The crustal extension estimates for the southern and central conjugate margin transects have been calculated taking into consideration the effect of the 7+ km/s high-velocity lower crustal body (LCB) for the calculation of the stretching factor. The LCB is seen in crustal-scale velocity models based on seismic refraction data (e.g., Breivik et al., 2009; Mjelde et al., 1996, 2005; Voss & Jokat, 2007). We considered two end-member scenarios with different amount of magma addition (0% and 100%). For the 0% magma addition, the LCB could be considered as fully crustal rock, while for the 100% magma addition, the LCB is considered as 100% magma underplating.

The current study also tests through a simplified version of fault population analysis whether brittle extension measured from the seismic interpretation on fault complexes along the Lofoten-Vesterålen margin is representative to the amount of extension experienced in the rifted conjugate margin setting (e.g., Reston & McDermott, 2014). The analysis (following methodologies described in Ackermann et al., 2001; Gómez-Romeu et al., 2020; Pickering et al., 1996; Walsh et al., 1991) determines the proportion of faults which have too small displacements to be imaged by conventional seismic reflection data. Extensional faults with larger throws (>0.2–0.5 s twt) are one of the most direct means by which continental lithosphere extends because they are readily visible on seismic data. However, the stretching of the whole lithosphere is far greater than that observed in faults within the upper crustal levels and where sedimentary basins rest (e.g., Kusznir & Karner, 2007; Mohn et al., 2015; Reston, 2005). Therefore, fault population analysis is employed to address such extension discrepancy, and to compare the magnitude of extension between the upper crustal levels and the whole continental lithosphere of the Lofoten-Vesterålen and NE Greenland margins. At the end, we account for possible geological processes responsible for the extension leading to breakup in the studied portions of the NE Atlantic.

4 | RESULTS

In this section we present estimates of brittle continental crustal extension and of stretching factors from seismic sections across the WRHFC and NURFC fault complexes utilizing the six selected MCS profiles within the LVM (Figures 4 and 5; Tables 1–3). In addition, continental crust extension estimates measured from the three pairs of updated conjugate transects are provided (Figure 6).

4.1 | Calculation of extension from fault components

4.1.1 | West Røst high fault complex

Updated seismic interpretation has resulted to the refinement of the main Late Mesozoic-Early Cenozoic rift phases within and in the vicinity of the WRHFC, and these are evidenced by six mapped fault stages (Tsikalas et al., 2019). The calculated extension derived from fault heave and

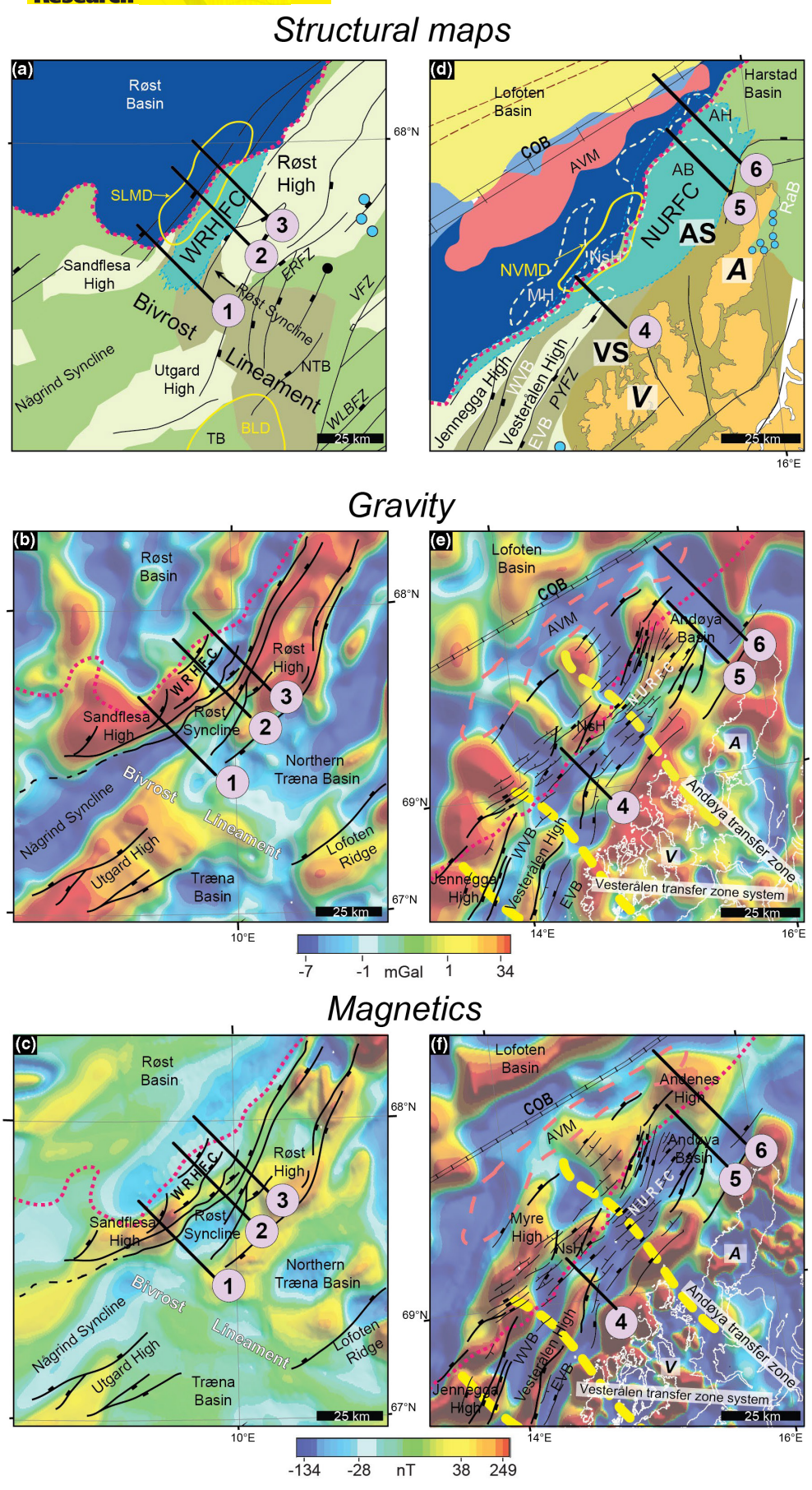

FIGURE 3 Zoomed portions on the focus study areas (structural maps) along the LVM and in the vicinity of the two fault complexes (a,d; WRHFC and NURFC). Gravity (b,e) and magnetic (c,f) anomaly data within same areas are shown. Seismic profiles (1–6), faults (in black lines; e.g., Meza-Cala et al., 2021; Tsikalas et al., 2019) and transfer zones (yellow dashed-lines; e.g., Meza-Cala et al., 2021) are also indicated. Other abbreviations and legend-features as in Figure 1.

displacement for each of the rift phases are ascribed to different main fault stages that represent the sequences affected by active time of faulting (profiles 1–3, Figure 4 and Table 1). The six main fault stages that have been mapped within the WRHFC include the Cenomanian–Turonian, Coniacian-Santonian, Campanian, Maastrichtian, Maastrichtian-Palaeocene, and Palaeocene fault stages. The summed fault heave and fault displacement ranges for each fault stage are indicated in Table 3.

Fault heave and fault displacement summation for the individual fault stages exhibit, in general, a decrease of the values towards the northern parts of the WRHFC (Table 1). Total cumulative fault heave and displacement estimates are, respectively, ca. 18 and 19 km in the southern parts of the WRHFC, whereas they become ca. 13 and 15 km in the northern parts of the fault complex. Overall, the Cenomanian–Turonian and Campanian fault stages are the ones contributing the most to the observed extension, whereas the fault stages inferred to contribute the least to extension is the Maastrichtian-Palaeocene fault stage. The Campanian fault stage is the most dominant in the southern part of the WRHFC, and gradually becomes less intense towards the northern parts of the fault complex. At the latter location, it is the Cenomanian–Turonian and the Coniacian-Santonian fault stages that exhibit greater fault heave and fault displacement magnitudes in comparison to the Campanian fault stage. From the remaining fault stages, the Maastrichtian stage is the most dominant, followed by the Palaeocene and Maastrichtian-Palaeocene fault stages (Table 3).

The average estimates of β_f for the different fault stages are provided in Table 3. A gradual increment in the average stretching factors is observed from Cenomanian–Turonian to Campanian fault stages with a local maximum of ca. 2.3. Moreover, the average stretching factor for the Maastrichtian fault stage shows a significant drop with a value close to ca. 1. For the Maastrichtian-Palaeocene fault stage, the average stretching factor is increased and is close to ca. 2. Hence, an oscillatory behaviour is observed within the WRHFC, but with an overall increasing trend from Late Cretaceous to Palaeocene. Eventually, the average stretching factor reaches its global maximum of ca. 2.7 at the Palaeocene fault stage. The increment in the recorded values of stretching factors measured from fault-block geometries for the last two fault stages in the WRHFC close to the time of continental breakup reflects the prominent intensity of the Late Cretaceous–Palaeocene rifting within the LVM.

4.1.2 | North Utrøst ridge fault complex

Late Mesozoic-Early Cenozoic rifting phases have been recently established and refined within and in the vicinity of the NURFC (Meza-Cala et al., 2021). Similar to the WRHFC, the calculated extension from fault heave and displacement from each main sequence affected during active time of faulting are ascribed to different fault stages interpreted in the NURFC (profiles 4–6, Figure 5 and Table 2). Four fault stages have been mapped within the NURFC and include Albian-Cenomanian, early Late Cretaceous, Late Cretaceous to latest Cretaceous–Palaeocene, and Palaeocene fault stages. A more detailed line-drawing interpretation was carried out in part of profile 4 (Figure 5 part of profile 4 close-up) in order to show the distinction of a mid-Cretaceous rift phase (Albian-Cenomanian fault stage) seismic marker prior to the initiation of the composite and more intensive Late Cretaceous–Palaeocene deformation. Note that it was not possible in the available seismic profiles (optimally illustrating the entire extent of NURFC) to differentiate separately between Late Cretaceous (Coniacian-Santonian–Campanian) and latest Cretaceous (Maastrichtian)-Palaeocene fault stages, thus these were treated together.

The outcome of the seismic and structural analysis shows a progressively increasing fault heave and displacement intensity starting with the Albian-Cenomanian fault stage, escalating to the early Late Cretaceous fault stage and the composite Late Cretaceous to latest Cretaceous–Palaeocene fault stage, prior to a distinctive drop at the Palaeocene fault stage (Table 2). The summed fault heave and fault displacement ranges for each fault stage are indicated in Table 3. The total cumulative fault heave and fault displacement estimates are, respectively, ca. 3 and 4 km in the southern parts of the NURFC, whereas they reach as much as ca. 5–6 and 7–8 km in the northern parts of the fault complex (Tables 2 and 3). Thus, extension in the southern part of the fault complex is mainly accommodated by the Palaeocene fault stage, whereas towards the northern part of the fault complex extension is mainly accommodated by the Late Cretaceous fault stages and less by the Palaeocene one.

Stretching factors from observed fault geometry (β_f) within the NURFC (Figure 5) were calculated in few

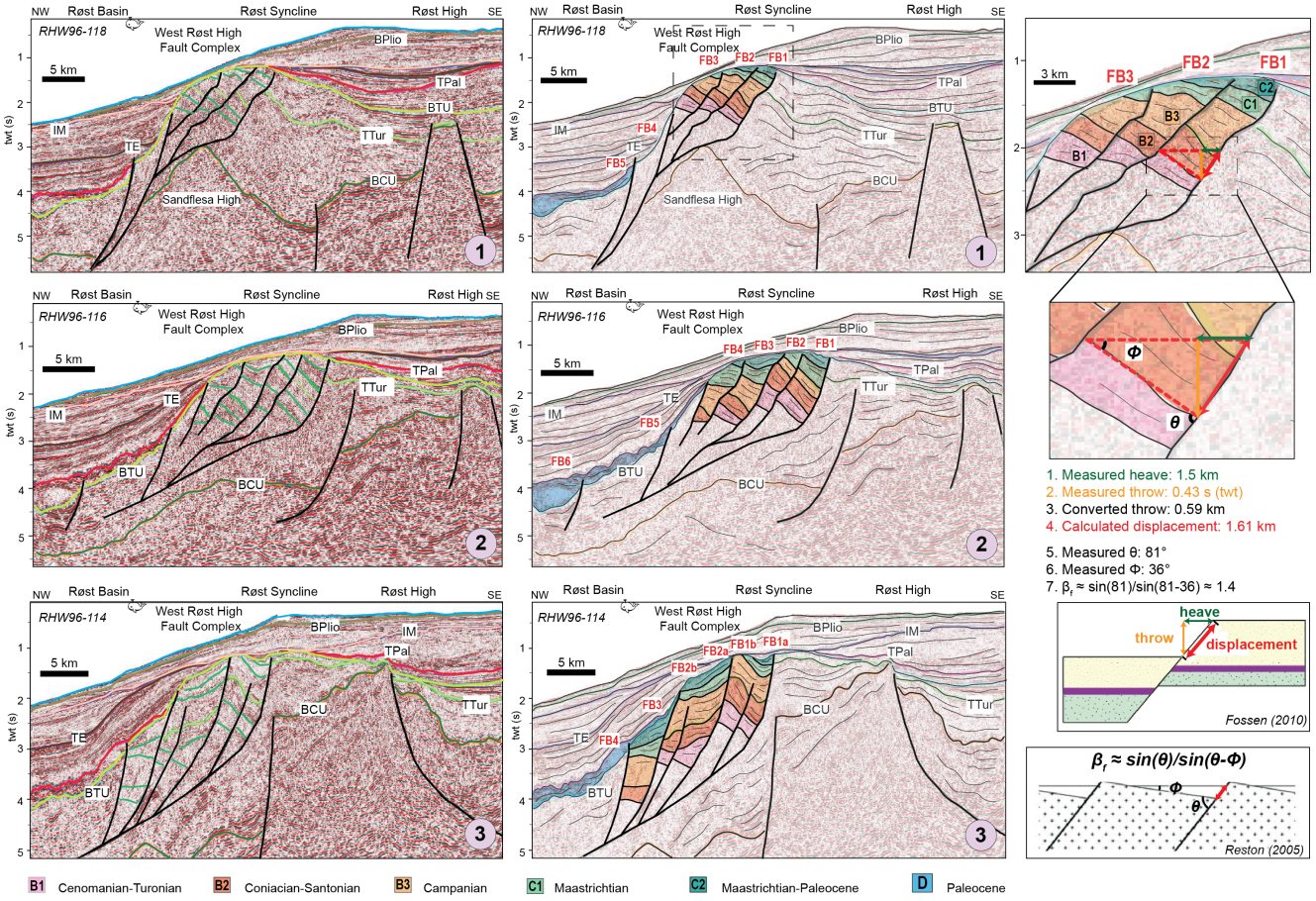

FIGURE 4 Seismic reflection profiles 1 to 3 along the West Røst High Fault Complex (WRHFC). Left-column: mapping of main stratigraphic seismic horizons/sequences and structural features in the WRHFC and its vicinity (e.g., Tsikalas et al., 2019; Figure 2). Middle-column: line-drawing interpretations and mapping of the distinct Late Cretaceous to Palaeocene seismic units (Figure 2) within the WRHFC. A set of different fault blocks (FB) constituting the low-angle detachment fault complex on the seismic profiles are also indicated and numbered. Right-column: fault-component-measurements approach and extension estimates' workflow. Distinct rotated reflections within each fault-block were associated to the different interpreted fault stages. The utilized workflow/procedure is indicated by the numbered steps (1–7) and explained in detail in the the text on chapter "3. Data and Methods". Profile locations indicated in Figure 1. Seismic horizon and seismic sequences (S1–S7) abbreviations as in Figure 2.

rotated fault-blocks following the same approach as for the WRHFC and are presented in Table 3. The observed trends/behaviour of the measured stretching factors for the different identified fault stages within the NURFC is slightly different compared to that of the WRHFC. Although the reduction from six to four identified fault stages in the NURFC with respect to the WRHFC is due to the progressively less detailed stratigraphic control from south to north, the stretching factor values from the mid-Cretaceous (Albian) to Late Cretaceous–Palaeocene fault stages show a continuous gradual increase within the NURFC. This contrasts with the oscillatory trend (but with an overall increment) observed in the WRHFC. In particular, the β_f estimates for the different fault stages do not exceed ca. 1.5, with the composite Late Cretaceous to latest Cretaceous–Palaeocene fault stage exhibiting the highest value (Table 3). However, the Palaeocene fault stage reaches a β_f as much as ca. 1.7 at the northwestern parts of the fault complex and represents the highest estimated stretching factor within the NURFC (Table 3). The obtained stretching factors, regardless the differences between the above-mentioned trends in both fault complexes, suggest an important contribution in the amount of extension within the LVM during the composite Late Cretaceous–Palaeocene rifting event.

4.2 | Calculation of extension for the entire continental crust

Figure 7 and Table 4 summarize the calculated extension on each crustal transect along the Lofoten-Vesterålen and NE Greenland conjugate margins. These results were obtained through the integration of their respective crustal

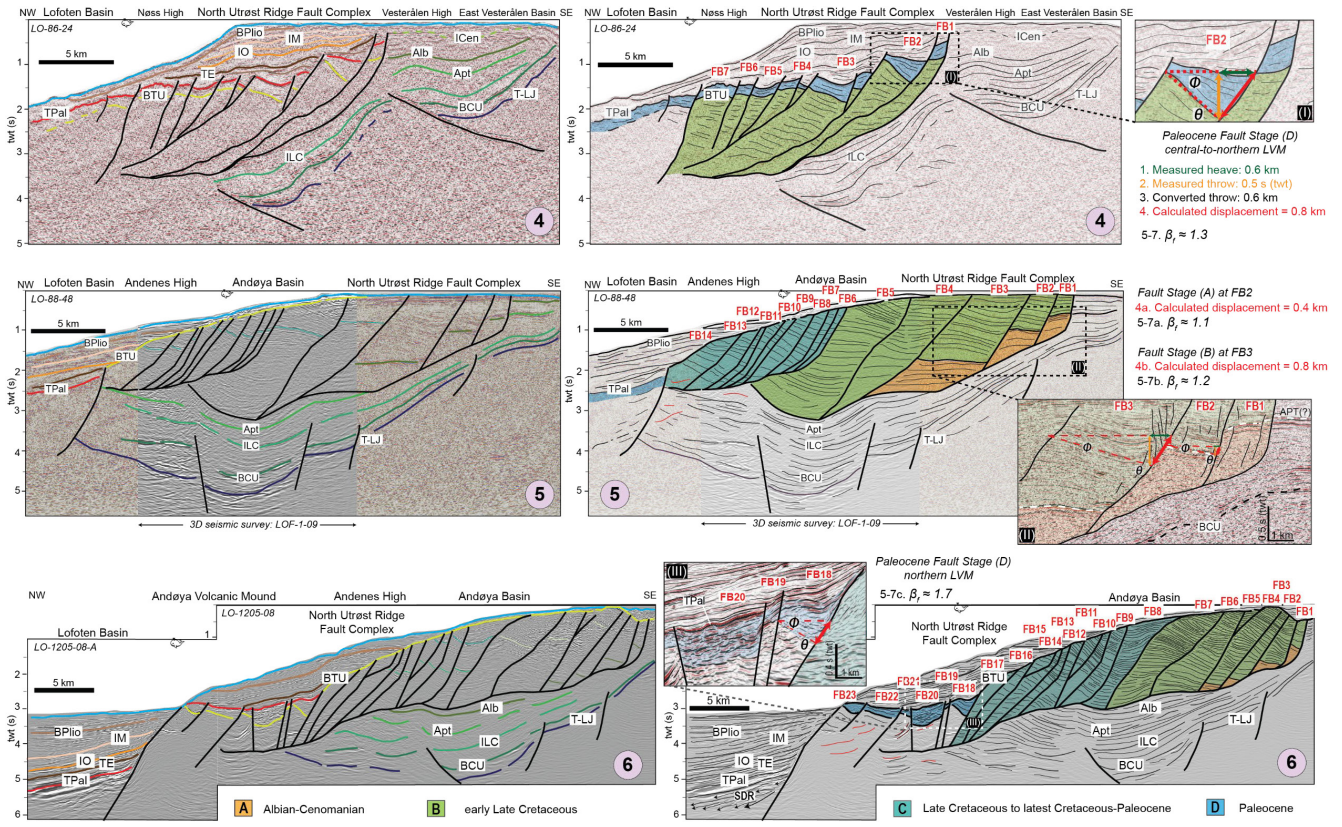

FIGURE 5 Seismic reflection profiles 4 to 6 along the North Utrøst Ridge Fault Complex (NURFC). Left-column: mapping of main stratigraphic seismic horizons/sequences and structural features in the NURFC and its vicinity (e.g., Meza-Cala et al., 2021; Figure 2). Right-column: line-drawing interpretations and mapping of the distinct Late Cretaceous to Palaeocene seismic units (Figure 2) within the NURFC. Similar to WRHFC seismic profiles 1 to 3, a set of different fault blocks (FB) constituting the low-angle detachment fault complex on the seismic profiles of the NURFC are also indicated and numbered. Inset (I): zoomed section of Palaeocene fault stage (D) within fault block 2 (FB2) on profile 4. Measurements of fault components, together with the derived extension and stretching factor (β_f) estimates are indicated by numbered steps following similar workflows/procedures as in Figure 4. Inset (II): extension (i.e. calculated displacement and β_f) for fault stages (A) and (B) within fault blocks 2 and 3 (FB2 and FB3), respectively. Inset (III): β_f for Palaeocene fault stage (D) within fault block 18 (FB18) on profile 6 offshore Andøya. Note the increment of β_f from south (offshore Vesterålen; profile 4) to north (profile 6). Profile locations indicated in Figure 1. Seismic horizon and seismic sequences (S1–S8) abbreviations as in Figure 2.

stretching/thinning factors derived from the crustal architecture illustrated in the updated transects (Figure 6). In all the analysed crustal transects, the stretching/thinning factors increase towards the continent-ocean boundary (COB). The variations in the magnitude of the stretching/thinning factors near the COB region correspond to the amount of magmatic addition (Table 4).

4.2.1 | Southern conjugate transect

The southern conjugate transect in the NE Greenland side (Foster Basin-Greenland transect) exhibits a current (final stretched) length of ca. 215 km, extending from mainland Greenland up to the defined COB location (Figures 6a and 7a1). The Foster Basin occupies the inner part of the transect (landward of the COB) and is interpreted as the seaward extension of the Late Palaeozoic to Mesozoic onshore basins (Figure 6a) (e.g., Corfu & Hartz, 2011). On the outer part of the transect (oceanward of the COB), the area is characterized by the occurrence of the Foster Volcanic Province, which consists of thick (2–4 km) volcanic flows (e.g., seaward dipping reflectors; SDRs) draped by Eocene and younger sediments (Figure 6a) (Reynolds et al., 2017). The Foster Volcanic Province has been classified as transitional crust by Voss and Jokat (2007), or as an oceanic plateau by Abdelmalak et al. (2017). The maximum thickness of the observed LCB that underplates the crust reaches ca. 20–25 km (Figures 6a and 7a1). The calculated stretching/thinning factors exhibit, as expected, a rather gradual eastward increment (Figure 7a2–a3). Considering a magma starving scenario (i.e. 0% magma addition), the average crustal extension is nearly ca. 30 km, whereas the average crustal extension in a full magmatic addition scenario (i.e. 100% magma addition) is as much as ca. 50 km (Figure 7a4 and Table 4).

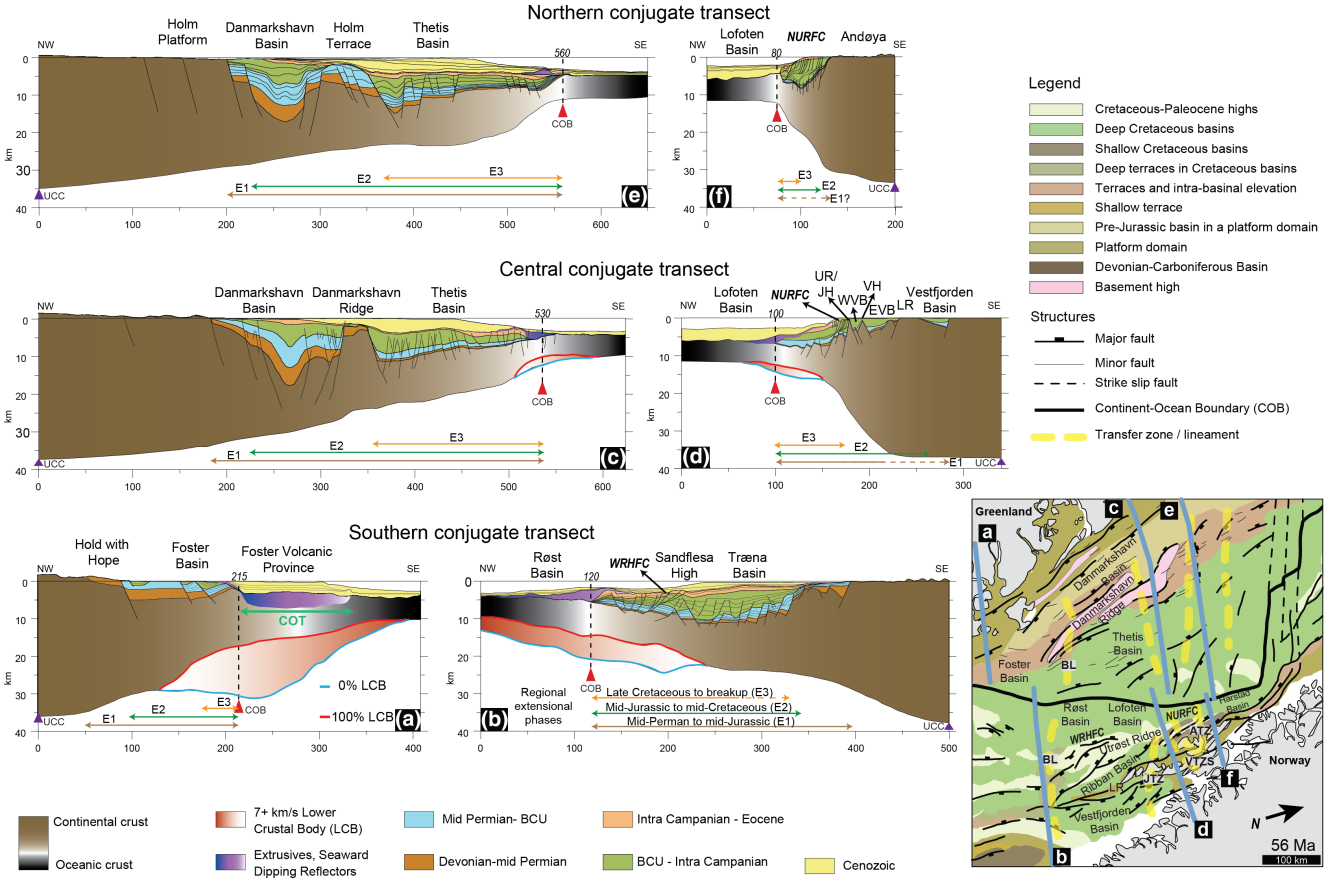

FIGURE 6 Paired conjugate crustal transects across the Lofoten-Vesterålen and NE Greenland conjugate margins illustrating the post-breakup crustal architecture and the extent of regional extensional phases (modified from Abdelmalak et al., 2022). Modelled underplating/magmatic addition (0% and 100% LCB scenarios) is illustrated only for the southern (a,b) and central (c,d) crustal transects, whereas no magma addition is modelled for the northern (e,f) crustal transects. The distance (in km) to the continent-ocean boundary (COB) with respect to the profile offset is indicated for each of the crustal transects. A continent-ocean transition (COT) zone is, in addition, indicated for the southern Greenland crustal transect (a). The transects were further used for estimations in crustal extension and stretching/thinning factors (Figure 7). Inset map: regional structure map of the conjugate setting restored prior to breakup and paired crustal transect locations. BCU, Base Cretaceous Unconformity; UCC, unstretched continental crust. Other abbreviations as in Figure 1.

In the Norwegian side, the current (final stretched) length of the southern transects (Bivrost Lineament-southern LVM transect) is approximately ca. 380 km, and includes a COB location that is defined at around ca. 120 km on the transect full-length (Figures 6b and 7a1). The sedimentary fill for most of the basin area ranges from Jurassic to lowermost Cenozoic sequences (Figure 6b). Minor packages of possibly Devonian?-mid Permian to Jurassic sedimentary units are present in the deeper parts of the basins (Figure 6b). Moreover, in the middle parts of the crustal transect (ca. 200 km-offset position) the southernmost part of the deformation directed by the WRHFC is evident (Figures 6b and 7a1), and there the crustal stretching/thinning factors show a continuous increment towards the COB location (Figure 7a2–a3). Oceanwards of the COB line, the transect depicts a considerable SDR wedge (ca. 3–5 km in thickness) in the outer part of the margin (Figure 6b). Similarly, the observed LCB does not exceed ca. 10 km, but extends over several hundreds of kilometres on the base of the crust (Figures 6b and 7a1). Considering a 0% LCB scenario, the average extension is as much as ca. 154 km, whereas for a 100% LCB case the average extension is ca. 170 km (Figure 7a4 and Table 4). Thus, these crustal extension estimates are more pronounced in the northernmost Vøring margin/southernmost LVM in comparison to the crustal extension estimates at the corresponding Greenland conjugate side (Figure 7a4).

4.2.2 | Central conjugate transect

The central conjugate transect in the NE Greenland side (Danmarkshavn Ridge-central Tethys Basin transect) exhibits a current (final stretched) length of ca. 350 km, and includes a COB location that is defined at

TABLE 1 Fault heave and displacement measurements for the West Røst High Fault Complex (WRHFC) based on seismic profiles 1–3 (P1–P3).

	Fault block			Measured heave (km)			Measured throw (s, twt)			Throw (km; converted)			Calculated displacement (km)			Cumulative heave (km)			Cumulative calc. displacement (km)		
Fault stage	**P1**	**P2**	**P3**	**P1**	**P2**	**P3**	**P1**	**P2**	**P3**	**P1**	**P2**	**P3**	**P1**	**P2**	**P3**	**P1**	**P2**	**P3**	**P1**	**P2**	**P3**
Palaeocene	4	5	2a	0.93	0.21	0.36	0.72	0.24	0.29	0.88	0.29	0.36	1.28	0.36	0.51	1.45	0.44	1.4	2.04	0.74	1.80
			2b			0.20			0.06			0.07			0.21						
	5	6	3	0.52	0.23	0.46	0.45	0.25	0.22	0.55	0.31	0.27	0.76	0.38	0.53						
			4			0.38			0.32			0.39			0.55						
Maastrichtian-Palaeocene	1	1	1a	0.76	0.28	0.24	0.23	0.15	0.12	0.28	0.18	0.15	0.81	0.33	0.28	1.32	0.79	0.99	1.39	0.95	1.26
	2	3	2a	0.56	0.28	0.48	0.13	0.15	0.36	0.16	0.18	0.44	0.58	0.33	0.65						
		4	3		0.23	0.27		0.13	0.15		0.16	0.18		0.28	0.33						
Maastrichtian	1	1	1a	0.90	0.21	0.21	0.32	0.12	0.19	0.44	0.17	0.26	1.00	0.27	0.34	2.32	1.50	1.51	2.48	1.75	2.20
	2	2	1b	1.18	0.31	0.35	0.22	0.14	0.33	0.30	0.19	0.45	1.22	0.36	0.57						
	3	3	2a	0.24	0.61	0.62	0.07	0.27	0.44	0.10	0.37	0.61	0.26	0.71	0.87						
		4	3		0.37	0.33		0.11	0.19		0.15	0.26		0.40	0.42						
Campanian	1	1	1a	1.78	0.72	0.30	0.36	0.40	0.22	0.50	0.55	0.30	1.85	0.91	0.43	4.47	3.59	2.37	4.68	4.07	2.92
	2	2	1b	1.45	0.85	0.55	0.29	0.32	0.35	0.40	0.44	0.48	1.50	0.96	0.73						
	3	3	2a	1.24	1.23	0.50	0.34	0.41	0.30	0.47	0.56	0.41	1.33	1.35	0.65						
		4	2b		0.79	0.43		0.24	0.14		0.33	0.19		0.86	0.47						
			3			0.59			0.18			0.25			0.64						
Coniacian-Santonian	1	1	1a	1.50	0.69	0.88	0.43	0.34	0.32	0.59	0.47	0.44	1.61	0.83	0.98	4.37	2.84	3.57	4.61	3.11	3.98
	2	2	1b	1.49	0.93	1.07	0.31	0.25	0.40	0.43	0.34	0.55	1.55	0.99	1.20						
	3	3	2a	1.38	0.90	0.57	0.32	0.24	0.16	0.44	0.33	0.22	1.45	0.96	0.61						
		4	2b		0.32	0.46		0.06	0.17		0.08	0.23		0.33	0.52						
			3			0.59			0.23			0.32			0.67						
Cenomanian–Turonian	1	1	1a	1.62	1.18	1.00	0.45	0.38	0.29	0.62	0.52	0.40	1.73	1.29	1.08	3.87	3.54	3.13	4.09	3.73	3.39
	2	2	1b	1.04	0.80	0.76	0.20	0.18	0.27	0.28	0.25	0.37	1.08	0.84	0.85						
	3	3	2a	1.21	1.56	0.92	0.30	0.25	0.18	0.41	0.34	0.25	1.28	1.60	0.95						
			2b			0.45			0.18			0.25			0.51						

Note: The fault components were measured for each of the identified fault stages interpreted within each fault block of the WRHFC (see Figure 2 and text for further details).

TABLE 2 Fault heave and displacement measurements for the North Utrøst Ridge Fault Complex (NURFC) based on seismic profiles 4–6 (P4–P6).

	Fault block			Measured heave (km)			Measured throw (s, twt)			Throw (km; converted)			Calculated displacement (km)			Cumulative heave (km)			Cumulative calc. displacement (km)		
Fault stage	**P4**	**P5**	**P6**	**P4**	**P5**	**P6**	**P4**	**P5**	**P6**	**P4**	**P5**	**P6**	**P4**	**P5**	**P6**	**P4**	**P5**	**P6**	**P4**	**P5**	**P6**
Palaeocene	1	–	18	0.10	–	0.30	0.08	–	0.24	0.10	–	0.29	0.14	–	0.42	1.99	–	1.01	2.60	–	1.36
	2		19	0.59		0.08	0.49		0.08	0.60		0.10	0.84		0.13						
	3		20	0.56		0.19	0.34		0.12	0.42		0.15	0.70		0.24						
	4		21	0.15		0.10	0.07		0.06	0.09		0.07	0.17		0.12						
	5		22	0.20		0.14	0.13		0.11	0.16		0.13	0.26		0.19						
	6		23	0.12		0.20	0.09		0.13	0.11		0.16	0.16		0.26						
	7			0.27			0.16			0.20			0.33								
Late Cretaceous to latest Cretaceous-Palaeocene	–	6	8	–	0.12	0.57	–	0.07	0.32	–	0.10	0.44	–	0.15	0.72	–	1.90	2.5	–	2.36	3.10
		7	9		0.11	0.17		0.05	0.11		0.07	0.15		0.13	0.23						
		8	10		0.18	0.26		0.11	0.14		0.15	0.19		0.24	0.32						
		9	11		0.35	0.19		0.2	0.09		0.28	0.12		0.45	0.23						
		10	12		0.13	0.18		0.10	0.12		0.14	0.17		0.19	0.24						
		11	13		0.17	0.19		0.1	0.1		0.14	0.14		0.22	0.23						
		12	14		0.05	0.21		0.05	0.11		0.07	0.15		0.09	0.26						
		13	15		0.16	0.34		0.1	0.13		0.14	0.18		0.21	0.38						
		14	16		0.63	0.2		0.2	0.11		0.28	0.15		0.69	0.25						
			17			0.19			0.1			0.14			0.23						
Early Late Cretaceous	1	1	1	0.12	0.11	0.08	0.09	0.09	0.09	0.12	0.12	0.12	0.17	0.17	0.15	0.64	2.19	2.21	1.03	2.98	2.79
	2	2	2	0.29	0.17	0.27	0.21	0.13	0.21	0.29	0.18	0.29	0.41	0.25	0.40						
	3	3	3	0.13	0.50	0.24	0.17	0.30	0.16	0.23	0.41	0.22	0.27	0.65	0.33						
	4	4	4	0.06	0.69	0.29	0.05	0.51	0.16	0.07	0.70	0.22	0.09	0.98	0.36						
	5	5	5	0.01	0.72	0.07	0.02	0.44	0.04	0.03	0.61	0.06	0.03	0.94	0.09						
	6		6	0.01		0.42	0.02		0.19	0.03		0.26	0.03		0.49						
	7		7	0.02		0.84	0.02		0.36	0.03		0.50	0.03		0.98						
Albian-Cenomanian	–	1	1	–	0.17	0.10	–	0.15	0.07	–	0.21	0.10	–	0.27	0.14	–	1.10	0.78	–	1.52	0.94
		2	2		0.28	0.22		0.23	0.1		0.32	0.14		0.42	0.26						
		3	3		0.65	0.27		0.38	0.11		0.52	0.15		0.83	0.31						
			4			0.19			0.1			0.14			0.23						

Note: The fault components were measured for each of the identified fault stages interpreted within each fault block of the NURFC (see Figure 3 and text for further details).

TABLE 3 Summary of cumulative fault heave and displacement, and average stretching factor measurements for both WRHFC and NURFC.

Fault stage	Cumulative fault heave range [km]		Cumulative fault displacement range [km]		Stretching factor [β_f]	
	WRHFC	NURFC	WRHFC	NURFC	WRHFC	NURFC
Palaeocene (D)	0.4–1.5	1.0–2.0	0.7–2.0	1.4–2.6	2.7	1.3; 1.7
Maastrichtian-Palaeocene (C2)	0.8–1.3		1.0–1.4		1.9	
Maastrichtian (C1)	1.5–2.3		1.8–2.5		1.2	
Late Cretaceous to latest Cretaceous-Palaeocene (C)		1.9–2.5		2.4–3.1		1.4
Campanian (B3)	2.4–4.5		2.9–4.7		2.3	
Coniacian-Santonian (B2)	2.8–4.4		3.1–4.6		2.1	
Cenomanian–Turonian (B1)	3.1–3.9		3.7–4.1		1.6	
Early Late Cretaceous (B)		0.6–2.2		1.0–2.8		1.2
Albian-Cenomanian (A)		0.8–1.1		0.9–1.5		1.1

Note: Stretching factors for Palaeocene fault stage (D) at NURFC represent two different estimates, one at its southern part (i.e. 1.3), and another at its northern part (i.e. 1.7). The fault component ranges are given for each of the interpreted fault stages within the fault complexes.

around ca. 530 km on the transect full-length (Figures 6c and 7b1). In the deep (ca. 20 km depth) Danmarkshavn Basin, Devonian-mid Permian to Upper Cretaceous sedimentary sequences constitute the main fill (Figure 6c). Towards east and into the central Tethys Basin, the Upper Palaeozoic strata are significantly reduced, whereas the Upper Mesozoic and Cenozoic units are present with considerable thickness expansion and constitute the main fill of the basin (Figure 6c). The calculated stretching/thinning factors exhibit an eastward gradual increment, yet they nicely illustrate the changes in top basement topography (Figure 7b2–b3). Both the SDR and lava flow wedges, and the underlying LCB are largely reduced in comparison to the southern crustal transect on the Greenland side (Figure 6a,c). Considering both 0% and 100% LCB scenarios, the average crustal extension estimates for both cases appear to be ca. 171 km (Figure 7b4 and Table 4). Furthermore, the calculated extension for the central transect on the Greenland side are larger in comparison to those of its southern crustal transect (Table 4).

The current (final stretched) length of the northern Lofoten/Vesterålen transect is approximately ca. 240 km and includes a COB location that is defined at around ca. 100 km on the transect full-length (Figures 6d and 7b1). The basin architecture observed at this part of the LVM is dominated by several elevated basin ridges/highs (e.g., Lofoten and Utrøst ridges), and with depocenters that are shallower in comparison to the basin-depths depicted at the south LVM transect (Figure 6b,d). In addition, the basins there exhibit little to almost none of the Upper Palaeozoic-Lower Mesozoic sedimentary sequences. Hence, the main fill is composed by Upper Mesozoic strata (Figure 6d). Moreover, in the northwest of both the crustal transect and of the Utrøst Ridge the onset of deformation is observed to be dictated by the NURFC (ca. 180 km-offset position; Figure 6d), and there the observed crustal stretching/thinning factors illustrate the corresponding increment due to the abrupt changes in Moho depth (Figure 7b2–b3). Towards the outer part of the margin and to the west of the transect, Cenozoic sedimentary successions represent the main infill into the Lofoten Basin, and they are deposited on top of a thinner wedge of SDR/lava flows in comparison to the volcanic wedges with the considerable thickness present in the south LVM transect (Figure 6b,d). Similarly, the observed LCB at the base of the crust is considerably less in thickness and areal extension (i.e. less magmatic volume overall in the central parts of the LVM). For both 0% and 100% LCB scenarios the average crustal extension estimates are ca. 63 and 66 km, respectively (Figure 7b4 and Table 4). These amounts of calculated crustal extension exhibit a reduction in magnitude

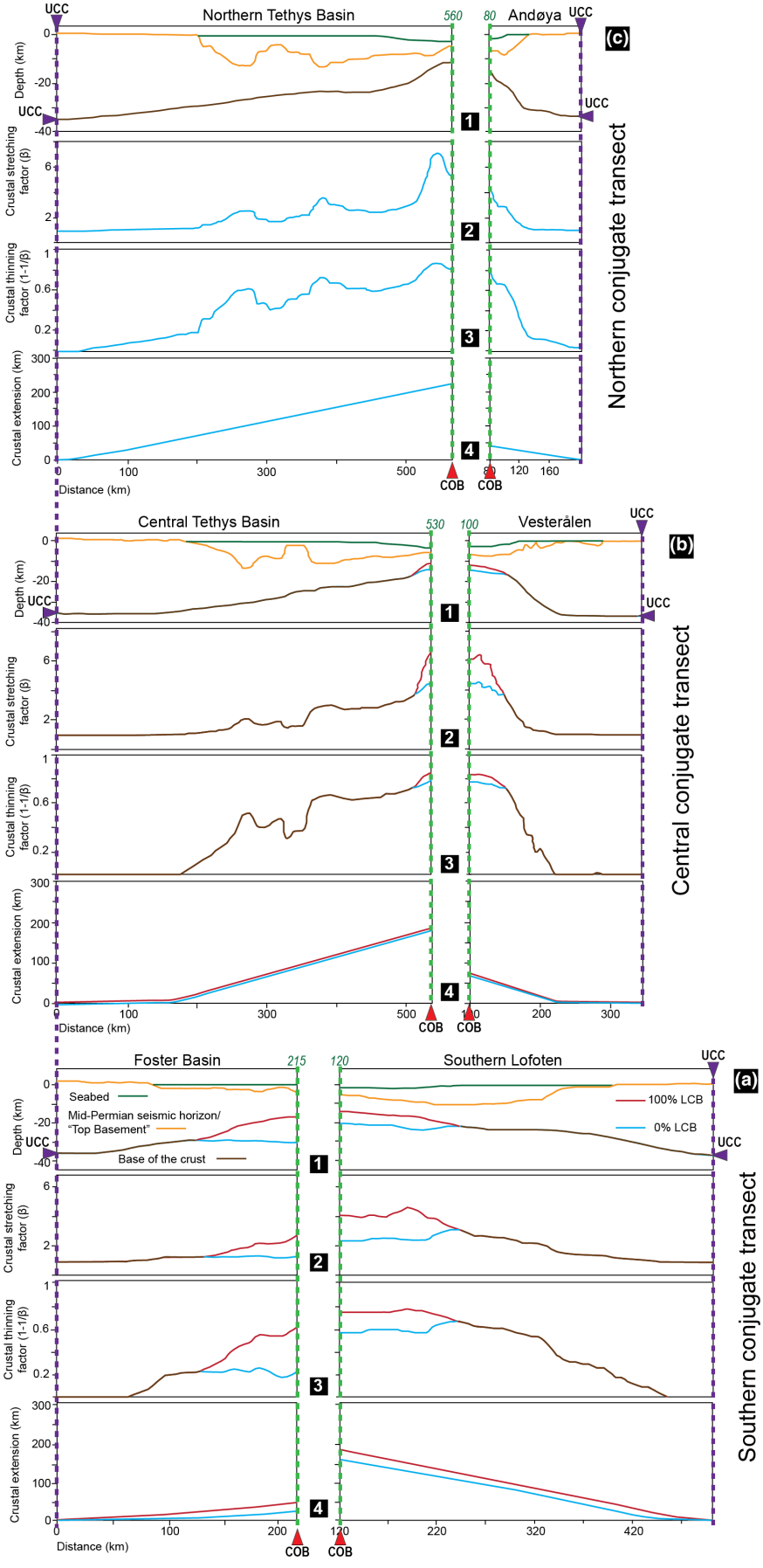

FIGURE 7 Crustal extension estimates for the southern (a), central (b), and northern (c) crustal transects. (1) Present crustal architecture showing bathymetry, top basement, Moho depth, and modelled underplating/magmatic addition (0% and 100% LCB scenarios). All crustal transects are plotted up to their respective COB location; (2) Stretching factor; (3) Thinning factor; (4) Calculated average crustal extension. Abbreviations as in Figure 6.

compared to the equivalent estimates in the south LVM transect and the conjugate central transect in Greenland (Table 4).

4.2.3 | Northern conjugate transect

The current (final stretched) length of the northern Danmarkshavn Ridge-northern Tethys Basin transect is approximately ca. 360 km and includes a COB location that is defined at around ca. 560 km on the transect full-length (Figures 6e and 7c1). In terms of basin architecture and sediment distribution, the margin characteristics are similar to those observed in the central transect on the Greenland side (Figure 6c,e). However, more of the mid-Permian to Upper Jurassic/lowermost Cretaceous sedimentary sequences are present in the northern Greenland transect (Figure 6e). The stretching/thinning factors exhibit an eastward gradual increase in magnitude, yet they nicely illustrate the corresponding changes in top basement topography (Figure 7c2–c3). Only a relatively small volume of SDR/lava flows wedge is interpreted for this transect, and there is no LCB observed below the crust (Figures 6e and 7c1). Thus, the estimated average crustal extension is ca. 226 km, and it represents the largest magnitude of extension estimates obtained for the studied portions of the NE Greenland margin (Figure 7c4 and Table 4).

The current (final stretched) length of the Andøya-northern LVM transect is approximately ca. 100 km and includes a COB location that is defined at around ca. 80 km on the transect full-length (Figures 6f and 7c1). At this part of the LVM, the basin architecture is even more distinctly different compared to both the southern and central LVM transects (Figures 6d,f). There are Cretaceous and possibly several mid/Upper Jurassic units that are the main sedimentary sequences composing the northern part of the LVM (Figure 6f). In addition, the NURFC and associated deformation is widely developed along most of the transect depocenter area and up to the COB (Figure 6f). In particular, the stretching/thinning factors exhibit a distinctive steep and abrupt increase near the associated deformation at NURFC location, and where it starts to propagate with a northwestward trend (Figure 7c2–c3). Oceanward from the COB location and into the Lofoten Basin, Cenozoic sedimentary sequences are seen to constitute the main infill (Figure 6f). Up to this part of the LVM, the wedge of SDR/lava flows is substantially depleted in comparison to the central LVM transect, and thus there is no LCB observed below the crust (Figures 6f and 7c1). Therefore, the estimated average crustal extension can be only as much as ca. 40 km, and represents one of the lowest crustal extension estimates in all the studied transects and within the LVM (Figure 7c4 and Table 4).

4.3 | Spatial distribution and correlation of fault stages to the Late Cretaceous–Palaeocene rift

Detailed seismic and structural interpretations have revealed the existence of different fault stages ascribed to distinct mid/Late Cretaceous–Palaeocene rifting pulses within and in the vicinity of the WRHFC and NURFC fault complexes in the southern and northern LVM, respectively (Figure 2; Meza-Cala et al., 2021; Tsikalas et al., 2019; this study). Specifically, parts of the Cretaceous to Palaeocene tectonism are better revealed in the WRHFC, whereas other parts of it are better illustrated in the NURFC, and it can be postulated that observations on the two fault complexes are complementary (Figure 8). Based on both the WRHFC and NURFC fault geometries and structural behaviour, their relative position within the margin, and the age of seismic sequences involved in the faulting, we assumed a similar and contemporaneous deformation mechanism operating along the study area was responsible for the formation of these structures. Faults within the WRHFC and NURFC are steep in the upper part of the fault complexes and sole out in the deeper parts at one or more detachment planes. These faults are believed to have initiated as steep planar (ca. 60°) normal faults that became listric and then low-angle (<17°) with continuous faulting/extension. Internal rotation of the blocks and inclination of fault planes were affected by the presence of underlying rift topography (Figures 2, 4 and 5).

Seismic and structural correlations indicate that the Albian-Cenomanian (A) fault stage is present in a larger extent towards the southern parts of the NURFC, and it is interpreted as an early faulting stage within the fault complex (Figures 5 and 8a,b). Similarly, a Cenomanian–Turonian (B1) fault stage is interpreted to be present in the WRHFC and ascribed as the initial phase of the deformation experienced by this fault complex in the southern LVM (Figures 4 and 8a,b). Following the later phase, less intense Coniacian-Santonian (B2) and Campanian (B3) fault stages are interpreted towards the southern parts of the WRHFC, as they become more prominent and dominant towards the northern parts of the fault complex (Figures 4 and 8a,b). Distinction of these later phases was not possible within the NURFC; nonetheless, an early Late Cretaceous (B) fault stage is interpreted there and can be correlated with the Cenomanian–Turonian to Campanian (B1 to B3) fault stages identified in the WRHFC (Figures 5 and 8a,b). This is because these fault stages represent the main initial structuring with affinity to both fault complexes in the respective portions of the LVM. The early Late Cretaceous (B) fault stage in the northern LVM and the B1 to B3 fault stages in the southern LVM are all characterized by wider (in extent) fault-blocks in the eastern

TABLE 4 Summary of estimated crustal extension for crustal transects across the Lofoten-Vesterålen and NE Greenland conjugate margins (Figure 6).

		Crustal stretching factor (average) [β_c]			Crustal extension (average) [km]		
Transect	**Zone**	**0% LCB**	**100% LCB**	**Stdr.**	**0% LCB**	**100% LCB**	**Stdr.**
N	Andøya-northern LVM	1.87	–	–	40	–	–
	Northern Danmarkshavn Ridge-northern Tethys Basin	2.19	–		226	–	
C	Northern Lofoten-Vesterålen	1.90	2.16	0.13	63	66	3
	Central Danmarkshavn Ridge-central Tethys Basin	1.84	1.87	0.02	170	171	6
S	Bivrost Lineament-southern LVM	1.95	2.40	0.19	154	170	7
	Foster Basin- Greenland	1.17	1.42	0.13	29	49	10

Note: The estimated average values of crustal stretching factor and extension are given for the different underplating/magma addition scenarios (0% and 100% LCB). The letters N, C, and S stand for northern, central, and southern crustal transects, respectively.

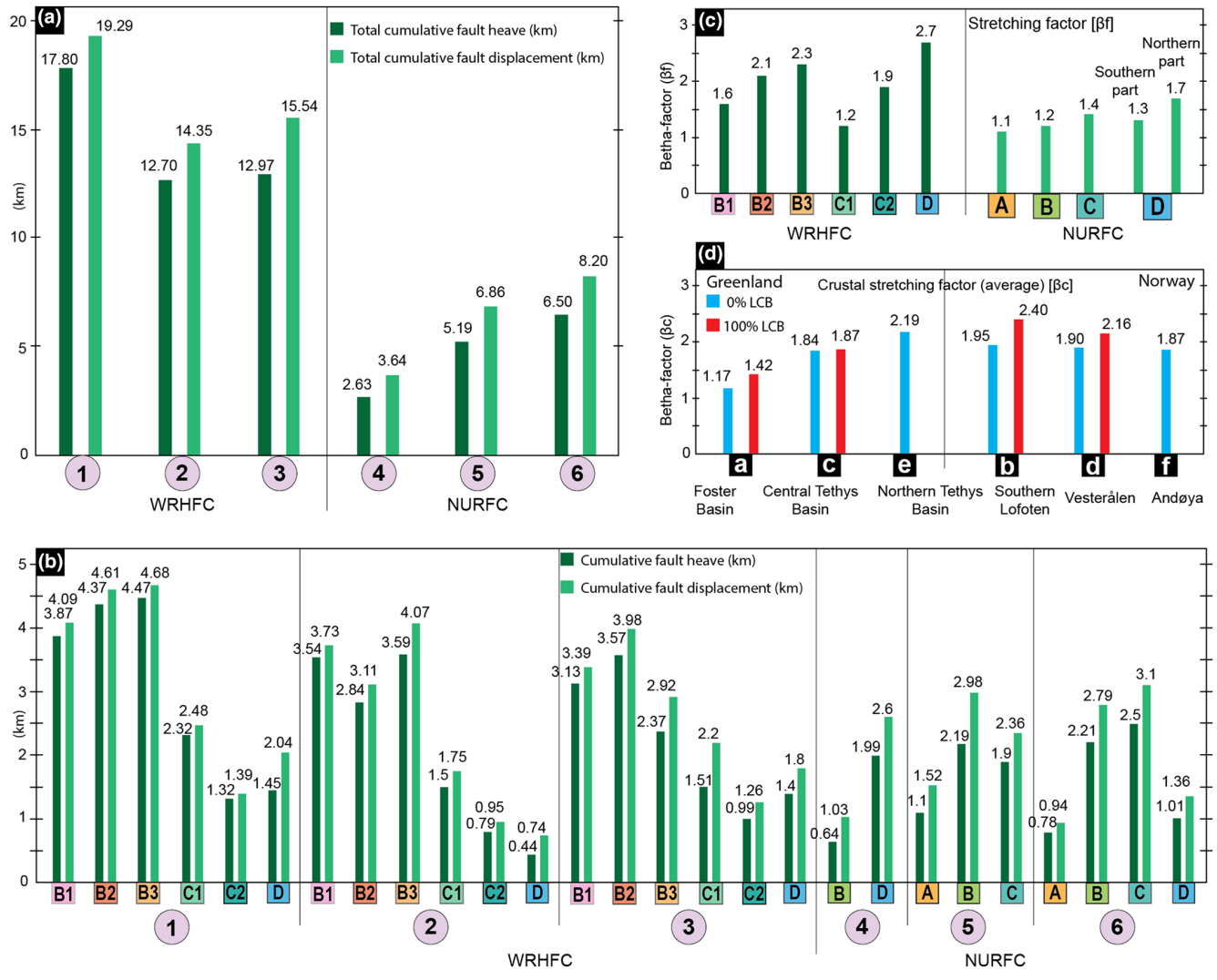

FIGURE 8 Summary of the calculations of extension and stretching factors (Tables 1–4). (a) Total cumulative fault heave and displacement (in km) derived from fault component measurements for each selected seismic profile (1–6). (b) Cumulative fault heave and displacement (in km) per fault stage (A, B, B1–B3, C, C1–C2, D) in each seismic profile. (c) Stretching factors derived from fault block geometries (β_f) and per fault stage. (d) Crustal stretching factors (average) derived from the conjugate transects architecture (β_c) considering different magma addition scenarios (0% and 100% LCB).

parts of the fault complexes (Figure 4). Similarly, there is involvement of thicker sedimentary units in the corresponding hanging blocks (Figures 3 and 5), together with the development of the décollement/detachment surface at slightly deeper levels (Tsikalas et al., 2019).

Towards the western parts of the WRHFC, the Maastrichtian (C1) and the composite Maastrichtian-Palaeocene (C2) fault stages are identified and possibly suggest either the initiation of a distinct rifting phase or the continuation of an earlier extensional event with more intensity in deformation than before (Figures 4 and 8a,b). These fault stages (C1 and C2) towards the northern parts of the LVM and within the NURFC have been treated as an extensive Late Cretaceous to latest Cretaceous–Palaeocene (C) composite fault stage (Figures 5 and 8a,b). This composite fault stage at NURFC is interpreted to be the result of a rift phase with more intense faulting, narrower in extent fault-blocks that reflect westward migration of rift activity, together with the décollement/detachment surface developing at shallower levels. In addition, minimal offset of the BTU seismic horizon is observed on top of these structures (Meza-Cala et al., 2021; Figures 5 and 8a,b). Due to the similarities in character, intensity and location of deformation imposed by fault stage (C) within the NURFC, both the C1 and C2 fault stages within the WRHFC can be correlated as contemporaneous to those and possibly share similar tectonic origins (Figure 2). A final rift phase close to the time of continental separation is manifested in both the WRHFC and NURFC fault complexes as the Palaeocene fault stage (D) (Figure 8a,b). This fault stage is characterized by newly formed and steep faults located towards the westernmost parts of the fault complexes and into the outer margin offsetting considerably the BTU horizon, together with cross-cutting relationships with the earlier developed Late Cretaceous low-angle detachment surface(s) (Figures 4 and 5). In addition, reactivation of some faults in the NURFC has led to the development of sediment wedges on the upper parts of this fault complex, that are linked to the Palaeocene fault stage (D) (Figure 5). Probably one of the most remarkable characteristics of this fault stage is that several of them are within the landward boundary of breakup lavas, and they are observed preventing the landward lava flow farther eastward on top of the WRHFC and NURFC fault complexes (Figures 4 and 5).

4.4 | Fault population analysis

The applied fault population analysis in this study consists of statistical expressions of power-law and exponential distributions of the sampled fault heave estimates from Figures 4 and 5 (Tables 1 and 2). Figure 9a shows a generalized example of the method as a cumulative frequency analysis with sampling artefacts related to a limited sampling area (data censoring) and to non-imaged faults below seismic resolution (data truncation). The idealized fault distribution shown by the cumulative frequency analysis consists of a central steep segment with negative gradient and represents the average fault population. The slope of a power-law distribution curve gives the fractal dimension and is usually between −0.7 and −0.9 suggesting that a portion of faults is not being seismically observed, whereas an exponential distribution type indicates that most faults are being seismically observed (Figure 9a). The analysis has been performed individually for both the WRHFC and NURFC fault complexes and we have grouped all the measured fault heaves from the corresponding seismic profiles in order to deduce more general observations about these tectonic-related structures (i.e. seismic profiles 1–3 and seismic profiles 4–6, respectively; Figures 4 and 5).

Figure 9b,c show the obtained results from the fault population analysis of all the interpreted faults/fault stages within the WRHFC and NURFC. The analysis demonstrates, in general, that the sampled faults of both fault complexes fit better with an exponential distribution. However, the behaviour of the faults at larger values of heaves in the data censoring area appears to be mostly above the predicted (exponential) frequency curve, and not below as expected by the method. Thus, the misfit suggest that a power-law frequency distribution needs to be considered (Gómez-Romeu et al., 2020). As a result, the value of the slope (red-line in Figure 9b,c), or the fractal dimension obtained for both the WRHFC and NURFC is approximately −0.8. Such value implies a lower-limit of resolution of ca. 150 and 80 m in order for faulting to be recognized on seismic data within the WRHFC and NURFC, respectively (i.e. data truncation in Figure 9b,c; Pickering et al., 1996). Hence, only ca. 11% and 13% of the extension through the interpreted fault geometries would be seen in the studied seismic profiles on the WRHFC and NURFC, respectively (Figure 9d).

5 | DISCUSSION

In this section we integrate the observations on the distinct rift phases and fault stages identified in the WRHFC and NURFC fault complexes in order to account for the multiphase tectonic evolution within the LVM towards breakup that led to the present asymmetry in the conjugate margins (Figure 6). We summarize our results and compare the amount of both the brittle crustal extension

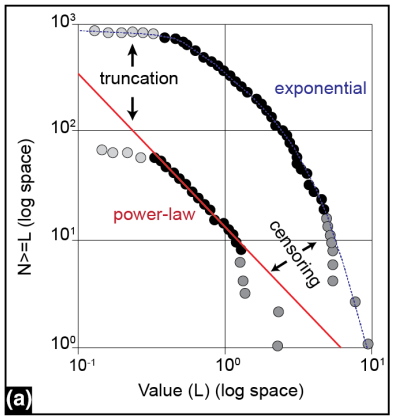

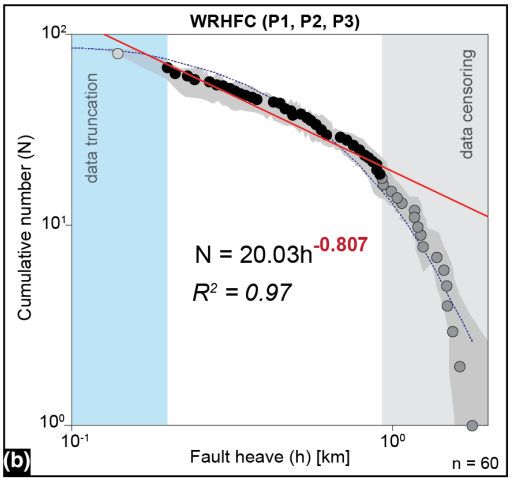

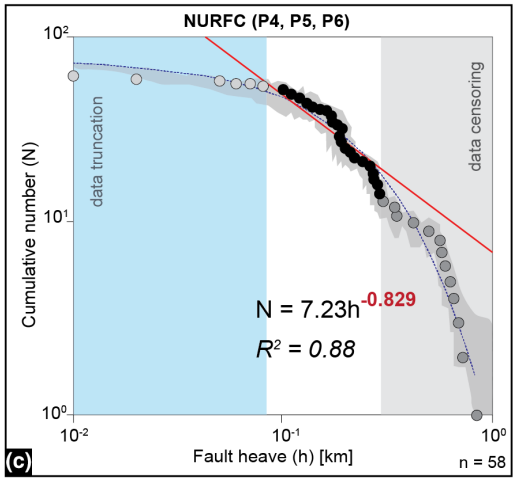

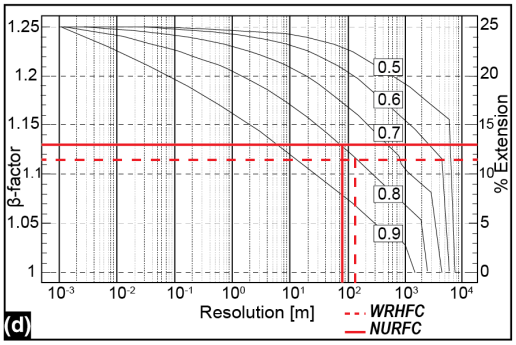

FIGURE 9 (a) Fault population plot showing power-law and exponential cumulative frequencies against fault size (measured as length, L) and sampling artefacts from truncation and censoring (redrawn from Ackermann et al., 2001). (b,c) Fault population analysis showing cumulative number (N) versus all the measured fault heaves (h, km; Tables 1 and 2) in this study from seismic interpretation of profiles 1 to 6 (Figures 4 and 5). Possible fits to power-law and an exponential relationship are shown. The fractal dimension for the power-law fitting is the exponent in bold-red of the equations. Regions representing data truncation and censoring are indicated in the plots, together with error envelopes (shading around fault heave data points). (d) Graph of the proportional measured extension for the lower-limit of seismic resolution for different ideally power-law populations of faults (redrawn from Pickering et al., 1996), and coupled with the results from measurements from both the WRHFC and NURFC fault complexes.

and total crustal extension required to lead to continental breakup. A fault population analysis for the studied WRHFC and NURFC fault complexes is also conducted to explore possible occurrence of sub-seismic resolution faulting and to compare these observations with extension estimates for the entire crust. Finally, we discuss the role of the prominent low-angle detachment fault complexes along the LVM in the context of the change of mode of deformation towards breakup.

5.1 | Apparent magnitudes of extension derived from fault complexes

The brittle extension in the LVM is based on the integration of measurements of cumulative fault heave and displacement for each of the fault stages interpreted within the WRHFC and NURFC fault complexes (Tables 1–3; Figure 8). No mid-Cretaceous extension is evident and thus was not measured on the WRHFC, whereas a range of maximum extension of ca. 1.1–1.5 km is calculated for the Albian-Cenomanian (A) fault stage at the NURFC (Figure 8a,b and Table 3). Subsequently, maximum extension due to the Cenomanian–Turonian to Campanian (B1 to B3) fault stages ranges ca. 3.9–4.7 km, and when combined such values make up the largest extension estimates within the WRHFC (Table 3). Towards the northern LVM, the equivalent early Late Cretaceous (B) fault stage has recorded a range of maximum extension of ca. 2.2–2.8 km that reflects the strong early episodes of deformation within the NURFC and shows significantly larger extension in comparison to the previous weaker mid-Cretaceous extension event (Figure 8a,b and Table 3). The Maastrichtian (C1) and Maastrichtian-Palaeocene (C2) fault stages observed

in the WRHFC exhibit maximum extension estimates in the order of ca. 2.3–2.5 and 1.3–1.4 km, respectively (Table 3). The average stretching factor for the latest Cretaceous fault phase (C1) shows a significant drop with a value close to ca. 1, and this may reflect a pause in extension or the onset of a different event (Figure 8c). Moreover, the amount of extension shows a decrease in magnitude in comparison to the early Late Cretaceous fault stages (B1 to B3) that have been interpreted in the southern parts of the LVM and within the WRHFC (Figure 8b).

On the other hand, the contemporary rift phase recorded by fault stages C1 and C2 towards the north of the LVM is the Late Cretaceous to latest Cretaceous–Palaeocene (C) composite fault stage interpreted at NURFC, and it exhibits a range of maximum extension of ca. 2.5–3.1 km (Figure 8a,b). Although, and unlike the corresponding fault phases at the southern LVM, fault stage (C) displays a relative increase in magnitude of extension compared with its precedent early Late Cretaceous (B) stage (Figure 8a,b). Finally, the Palaeocene (D) fault stage developed near the time of continental breakup (Figure 2). The maximum extension estimates for this fault stage are in the order of ca. 1.5–2 and 2–2.6 km in the southern and northern LVM parts and within the WRHFC and NURFC fault complexes, respectively (Table 3). A possible explanation accounting for the observed reduced extension of the Palaeocene fault stage (D) may be the extensive Late Cretaceous–Palaeocene and post-Miocene erosion rates in the study area (e.g., Breivik et al., 2020) that led consequently to the removal of much of the evidence of deformation related to early Cenozoic (except the few sedimentary wedges still present on the upper parts of the NURFC; Figure 5), as well as the regional tectonostratigraphic role of the Bivrost Lineament in the area resulting in thin or even absent Cenozoic strata within the uplifted basement of the LVM (e.g., Maystrenko et al., 2017; Tsikalas et al., 2019, 2022). Despite the differences in absolute values, there are close similarities in the magnitude of extension (comparatively to progression in time) in the various fault stages/rift phases between the two fault complexes (Figure 8c). In general, it appears from our analysis that WRHFC has accommodated a relatively greater amount of focused and concentrated extension, whereas the NURFC has a much wider area with widespread extension intensity (Figure 8a).

5.2 | Crustal extension along the NE Atlantic margins

The resulting lateral asymmetry of crustal geometries of the conjugate margin counterparts depict a change in width along the transects with an increase in extension during Late Cretaceous–Palaeocene rifting, and reflects the vertical contrast between the crustal structure of the system (Figures 6 and 7). In particular, the LVM exhibits maximum crustal thicknesses in the order of ca. 23–26 km beneath the slope, while it thickens towards mainland Norway reaching a maximum of ca. 36 km (Breivik et al., 2017; Faleide et al., 2008; Faleide, Zastrozhnov, et al., 2022) (Figures 6 and 7). In the southernmost part of the Lofoten margin, the Moho depth is about 20 km, whereas it increases to about 27 km underneath the southern Utrøst Ridge near the shelf edge, to become shallower towards the outer margin (Mjelde & Sellevoll, 1993) (e.g., Figures 6b and 7a1). The Moho depth does not record/reflect the presence of mapped basement highs and basins on the LVM, probably because crustal extension within the LVM shelf area is not strongly affected by the continental breakup, and consequently the depths of the basins are relatively shallow (ca. 6 km deep) (Breivik et al., 2020) (Figure 6d,f). Additionally, the basin infill exhibits high density, which could reduce Moho topography underneath through isostatic adjustments (e.g., Tsikalas, Eldholm, et al., 2005) (Figure 7b1,c1). All the above processes may account to some degree for the observed crustal architecture and asymmetry between the Lofoten-Vesterålen and NE Greenland conjugate margins (e.g., Tsikalas, Faleide, et al., 2005). The latter is characterized by higher variations in crustal thickness and crustal densities, shallower maximum crustal depth (ca. 26 km), and deeper Mesozoic sedimentary basins (Fyhn et al., 2021) (e.g., Figure 6a,c,e).

For the case of the LVM and the nearby northern Vøring margin, the calculated average stretching factors and the integrated amounts of stretching for post mid-Jurassic times are, respectively, ca. 1.6 and 1.7 (max. value of ca. 3 and of 3.4) and ca. 70 and 127 km of extended crust (Skogseid et al., 2000). Similarly, a stretching factor of at least ca. 3 will explain the thin crust observed in the LVM at the onset of breakup (Breivik et al., 2017) (Figures 6 and 7). More specifically, estimates for the Late Cretaceous–Palaeocene total extension within the southern LVM yield a value of ca. 33 km, together with stretching factors exceeding ca. 2.7 at the COB (Skogseid, 1994) (e.g., Tables 3 and 4). Additionally, the Late Cretaceous–Palaeocene rift in the same area may have reached a total cross-margin width of 200–250 km (sum of rift widths on the conjugate mid-Norway and NE Greenland conjugate margins), and with comparable stretching mechanisms as those at the Vøring margin including depth-dependent lithosphere stretching and thinning (Tsikalas et al., 2008). The resulting less pronounced rifted width zone within the Lofoten-Vesterålen margin in comparison to the

greatly extended lithosphere beneath the adjacent Vøring and SW Barents Sea margins, and the conjugate East Greenland margin may have resulted from a combination of the final oblique rift axis, location of the COB, along-margin distribution of the LCB, and possibly far-field magmatic effects produced at the centre of the Iceland Plume (e.g., Abdelmalak et al., 2016, 2017; Faleide et al., 2008; Skogseid et al., 2000; Tsikalas et al., 2012). In addition, a general seaward increase in Cenozoic tectonic subsidence was also reported, reflecting the increased tectonic activity as the zone of final continental separation between Greenland and Norway was approached (Skogseid, 1994; Skogseid et al., 1992), and which is reflected by gradual increase in the stretching/thinning factors towards the line of continental separation (Figures 7 and 8; Tables 3 and 4).

The conducted measurements of crustal extension indicate a relative increase towards the southern LVM and the adjacent northern Vøring margin, whereas a northwards relative increase is present at the conjugate NE Greenland margin (Figure 8d; Table 4). Considering a scenario without magmatic underplating (i.e., 0% LCB), the derived cross-margin average total extension estimates along the southern, central, and northern crustal

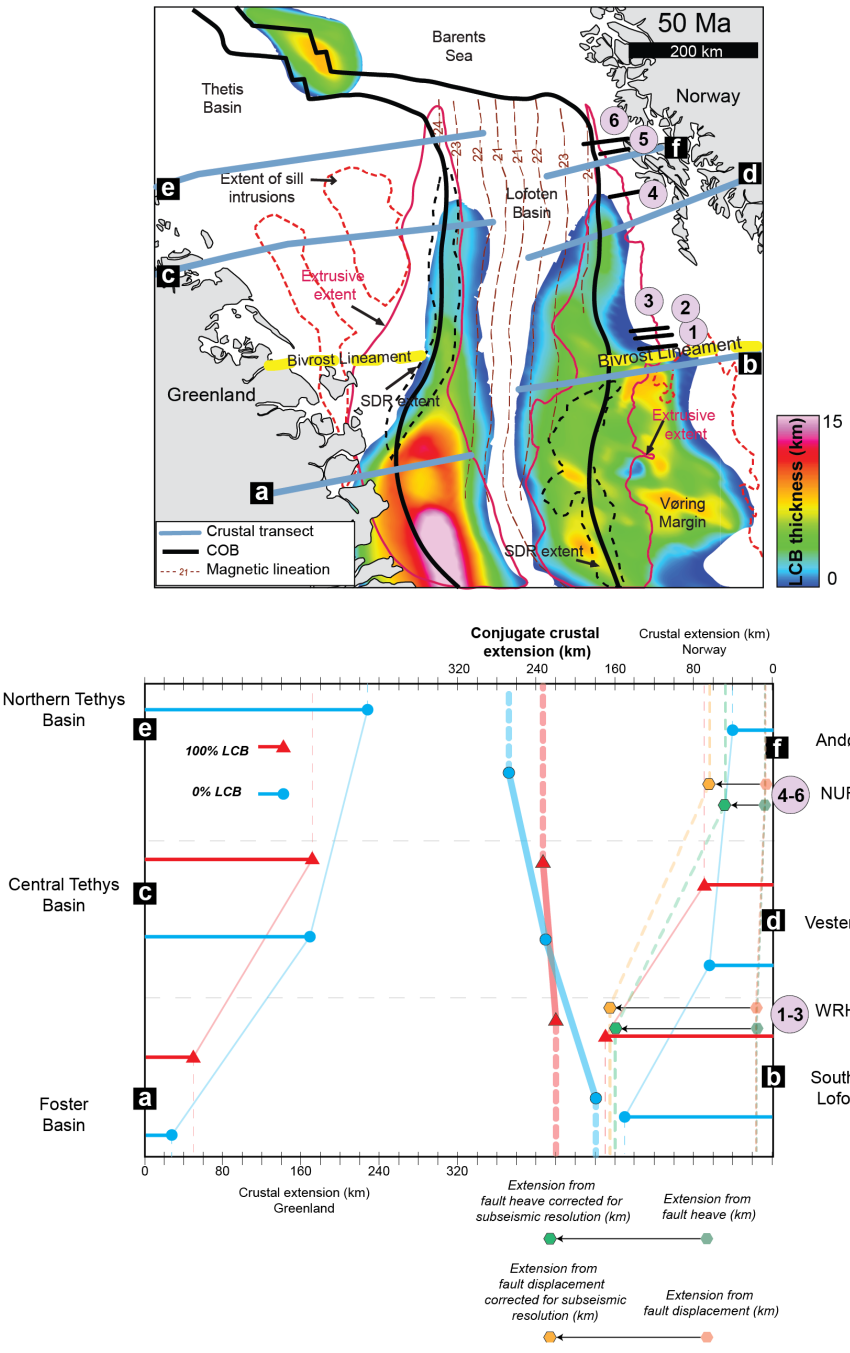

FIGURE 10 Summary of the magnitude of extension leading to breakup in the Lofoten-Vesterålen (LVM) and NE Greenland conjugate margins. Note the comparison of extension across the southern, central, and northern conjugate transects used in this study, together with those measured from the seismic profiles across the WRHFC and NURFC fault complexes (profiles 1 to 6) in the LVM. The correction for subseismic resolution faulting for extension measured on the seismic profiles across the fault complexes is also shown. The inset map illustrates the thickness (in km) of the modelled Lower Crustal Body (LCB) within the NE Atlantic conjugate margins (modified from Abdelmalak et al., 2017).

transects are ca. 183, 233, and 266 km, respectively (Figure 8d; Table 4). Similarly, considering a scenario with full magmatic underplating (i.e. 100% LCB), the derived cross-margin average total extension estimates along the southern and central crustal transects are ca. 219 and 237 km, respectively (Figure 8d; Table 4). This means that the larger the magma addition (i.e. LCB), the larger the crustal extension and their respective crustal stretching/thinning factors (Figures 7, 8d and 10). This is, particularly, more relevant for the southern LVM which lies in the vicinity to the northern Vøring margin, as the calculated crustal extension appears to be modulated by the thickness and distribution of a high-velocity (7+ km/s) LCB (Figures 6a,b and 7a). In the case of the Vøring margin, LCBs underplating the crust have been modelled from the outer parts of the area (e.g., Vøring Plateau) up to the extended continental crust where sedimentary basins lie (e.g., Någrind Syncline) (e.g., Gernigon et al., 2001, 2003; Lundin & Doré, 1997; Mjelde et al., 2007) (Figures 1 and 10). The LCB in that region is suggested to have a pre- and syn-breakup magmatic origin, and to have further influenced the faulting and distal development of the sedimentary basin at least 10–15 Ma prior to breakup (e.g., Abdelmalak et al., 2017; Gernigon et al., 2004). Our results reflect in a simple way the Late Jurassic and Late Cretaceous–Palaeocene β-factors spikes close to the COB and the more than ca. 150 km of pre-drift extension required for breakup along the Vøring margin (Wangen et al., 2011; this study) (Table 4 and Figures 6a, 7a, 8d). In comparison, no LCB is considered for the northern parts of the studied area, and the average crustal extension reaches only as much as ca. 40 km at the northern LVM, whereas in the northern parts of the NE Greenland margin crustal extension exceeds ca. 200 km (Table 4 and Figure 10). The LCB is thickest (12–15 km) just below the Foster Basin and the Foster Volcanic Province (Figures 6a and 10). If we count on the link between sill intrusion complex and the extent of the LCB, it could be possible to expect that the latter is present in the northernmost parts of the studied area (e.g., offshore Andøya and northern Tethys Basin), as well as covering greater areas such as in the southern parts of the Jan Mayen Ridge (Abdelmalak et al., 2017; Breivik et al., 2012).

5.3 | Corrected extension for sub-seismic resolution faulting in the context of crustal-scale rifting

The amount of extension from measured fault components within the WRHFC and NURFC fault complexes underestimate the amount of crustal extension (Figure 8c,d). Thus, it is important to include the corrected extension for sub-seismic resolution faulting (Table 5; Figure 10). The corrected extension derived from fault components in the WRHFC is between ca. 141 and 155 km (Table 5). Similarly, the Late Cretaceous–Palaeocene rift contributed to at least ca. 140 km of the extension observed within some portions of the NE Atlantic rift zone, which exceeds 300 km in width near the southern LVM area (Skogseid, 1994; Skogseid et al., 2000; this study). On the other hand, the corrected extension derived from fault components in the NURFC is between ca. 35 and 47 km (Table 5). Breivik et al. (2017) proposed a detachment model for the crust within the offshore part of Vesterålen islands using refraction data and suggested ca. 26–30 km of crustal extension. This is, in a general sense, comparable to our extension estimates for the central and northern parts of the study area (Figure 10). Overall, the conducted analysis for extension corrected for sub-seismic resolution faulting exhibits great similarities with reported values of extension for the different portions of the LVM, and it is in accordance with the extension measurements for the entire crust as no extension discrepancy is present (Figure 10 and Tables 4 and 5). The extension discrepancy and the apparent extension underestimation may result from differential compaction of sediments during and after rifting, non-uniform stretching of the lithosphere, rheological layering of the crust, and/or significant plastic/ductile deformation in the rock volume (Reston, 2009; Walsh et al., 1991). The rheological differentiation at depth in rifted margins favours non-brittle extension via depth-dependent stretching and thinning that result in upper lithosphere extension measurements being far less than the extension observed in the entire lithosphere within the proximal and necking domains (Davis & Kusznir, 2004) (Figure 8c,d). Alternatively, several studies have proposed that much brittle extension is undetected because of seismic imaging limitations caused by several

TABLE 5 Summary of brittle extension based on seismic profiles 1–6 (P1–P6; Figures 2 and 3) with correction for sub-seismic resolution faulting (see text for further details).

Fault complex	Total cumulative fault heave range (TFH) [km]	Total cumulative fault displacement (TFD) range [km]	Corrected TFH range [km]	Corrected TFD range [km]
WRHFC	13–18	15–19	118–164	136–173
NURFC	3–6	4–8	23–46	31–62

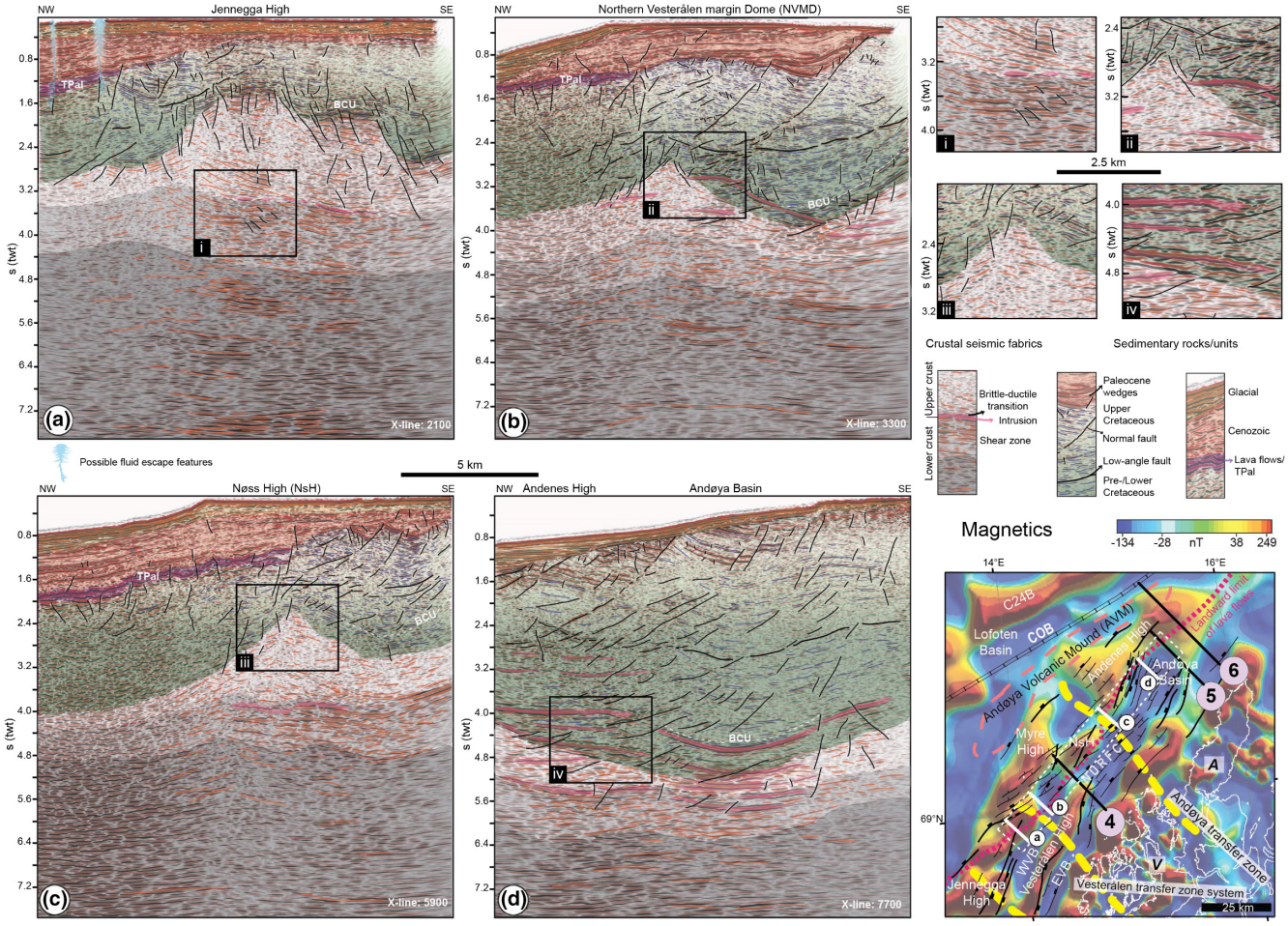

FIGURE 11 Seismic examples illustrating structural relationships between the North Utrøst Ridge Fault Complex (NURFC), the surrounding crust underneath and the Cenozoic units/features above (a–d). Seismic crustal fabrics, including an interpreted shear zone within the lower crust, as well as possible various degrees of coupling across the upper crust and the sedimentary units draping the basement is shown in the insets (i–iv). Note the variations from south to north of basement topography in the seismic examples and in the potential-field inset map (Magnetics), and how it modifies the fault geometries (listric vs. low-angle) and amplitude of deformation within the NURFC. Relative stratigraphic positions of the Base Cretaceous (BCU) and Top Palaeocene (TPal) seismic horizons is shown. Other features are also illustrated, including the spatial distribution of lava flows related to breakup with respect to up-domed portions of the NURFC such as the northern Vesterålen margin Dome (NVMD), and possible volcanic intrusions and fluid release features in the area. The seismic examples are from the 3D seismic survey LOF-1-09 (Figure 1). Both the extent of the 3D survey (dashed rectangle) and profile locations are indicated in the inset map.

factors, including: sub-seismic resolution or small-scale faulting (e.g., Marrett & Allmendinger, 1992; Ranero & Pérez-Gussinyé, 2010); mis-interpreted or unidentified fault geometries, such as rolling-hinge and detachment faults (e.g., Manatschal et al., 2001); and magmatic diking and underplating features that could also accommodate large amount of extension at the scale of the whole crust of the conjugate system through fault nucleation/reactivation and flexure (e.g., Phillips et al., 2018; Sun et al., 2019).

The fault population analysis employed in this study provides, in addition, a coefficient of determination (R^2), and it indicates for this case a good fit of the observed fault heave distribution to the theoretical statistical model (i.e. R^2 between 0.88 and 0.97; Figure 9b,c). Seismic interpretation supports the presence of more than one fault stage within the WRHFC and NURFC, and more than one power-law line can be fitted to better represent the different slope segments on the fault population graphs in Figure 9b,c. In this context, multiple rift phases from Late Cretaceous to Palaeocene could be interpreted for the development and evolution of both the WRHFC and NURFC in the LVM, similar to the cases in the Galicia margin (Reston, 2005) and in the northern Vøring margin (Zastrozhnov et al., 2018, 2020). Our results of corrected extension for sub-seismic resolution faulting are a good match to the amounts of crustal scale extension as the Lofoten-Vesterålen margin (as well as the NE Greenland side) becomes poorer in available magma content related

to breakup progressively towards the north (e.g., Gernigon et al., 2004; Lundin & Doré, 1997) (e.g., Figures 7c and 10). The significant distance away from the magmatic centre of the Iceland Plume, and the tectono-magmatic basin segmentation (i.e. Bivrost Lineament; Figures 1, 3 and 10) could have had an influence in the delivery of melt into the northern parts of the NE Atlantic (e.g., Doré et al., 1997; Schiffer et al., 2020). Moreover, the outer part of the Foster Basin corresponds to a still debated >100 km-wide continent-ocean transition (COT) zone interpreted as the seaward extension of the Late Palaeozoic to Mesozoic onshore basins (e.g., Dinkelman et al., 2010) (Figure 6a), and which could further affect calculation of extension in the region (Figure 10) (e.g., White et al., 2008). The lack in definition of a precise COB in that area is expected to potentially attenuate the measurements of crustal extension compared to the amount of extension observed in the conjugate side in Norway (e.g., Figure 7a). An increment in the magnitude of extension can be expected if the COB position is moved towards the south-eastern part of the Foster Basin (Figure 6a) because of an increment in the location of the distal limit of contiguous continental crust (e.g., Gómez-Romeu et al., 2020). Thus, the wider the margin, the greater the magnitude of calculated extension. Nonetheless, the greater difference between extension in the southern part of the Lofoten-Vesterålen margin, including the corrected extension for sub-seismic resolution faulting derived from the WRHFC, and its conjugate side in NE Greenland could be due to variations of amplitude and intensity of the different extensional events on the region, and to the difference in conjugate margin width constrained by the basin infill (e.g., Abdelmalak et al., 2022; Wangen et al., 2011) (Table 4 and Figures 6 and 10). Considering all these features and the discussion above, our corrected extension for sub-seismic resolution faulting is probably a representation of the mid-Cretaceous and Late Cretaceous–Palaeocene rifting, especially in the northern parts of the Lofoten-Vesterålen margin. On the contrary, more of the mid-Permian and Late Jurassic-Early Cretaceous rifting events are represented towards the southern parts of the studied region (Figures 6, 7 and 10).

5.4 | Ductile mode of extensional deformation towards breakup

The high extension rates during early Cenozoic observed along the Vøring margin have caused only minor faulting recorded on conventional seismic reflection profiles (Figures 7, 8d and 10) (Skogseid et al., 1992). This behaviour was attributed to ductile crustal deformation, mobilization of Cretaceous shales, and to breakup-related magmatic intrusions (Skogseid et al., 1992), which are features also observed within and in the vicinity of the WRHFC and NURFC (Figures 2, 4 and 5). Seismic anisotropy indicates inclined (45° dipping) structures in the lower crust across the Lofoten Ridge and Røst High (Mjelde & Sellevoll, 1993). These dipping features were further suggested to have resulted from post-Caledonian extensional episodes along faults reaching as deep as 10–15 km, and where they become low-angle at depth and conform a region with significant lateral ductile flow of material (Mjelde et al., 1996). Similarly, NNE–SSW trending and steep brittle faults that detach into low-angle shear zones or NW-oriented ductile bands that follow a comparable trend to Devonian detachments have been documented in the onshore part of Vesterålen (Wilson et al., 2006). New seismic observations on the basin configuration and crustal structures offshore Vesterålen and Andøya indicate the presence of a set of dipping and horizontal reflections suggesting the existence of a shear band such as the one offshore south Lofoten (Figure 11). The sheared region seen on seismic data affects the eastern edge of the necking domain (Tasrianto & Escalona, 2015), which consists of a NE–SW oriented ca. 90 km-long corridor that is situated just underneath the basement highs and is found at 3.5–4.5 and 5.5–6.5 s twt depths offshore Vesterålen and Andøya, respectively (Figure 11). Seismic reflection data are obscured below the lava flows and impede an interpretation of whether the sheared region within the crust could extend farther towards the COB region (Figure 11), yet the proposed crustal-scale detachment configuration offshore Vesterålen by Breivik et al. (2017) suggests that such structural feature may exist regionally within the studied region.

The listric or low-angle detachment geometries in the WRHFC and NURFC developed depending on whether the underlying basement relief is high or low, respectively (Meza-Cala et al., 2021; Tsikalas et al., 2019) (Figure 3). How basement relief is distributed can influence the coupling ability of later faults within shale-rich lithologies with deeper crustal-affinity deformation in the area (e.g., Claringbould et al., 2017), as well as the resulting fault geometries (Osmundsen & Péron-Pinvidic, 2018) (Figures 2 and 11). In addition, the observed rift topography and faulting character along the Lofoten-Vesterålen margin have been suggested to vary in response to the presence of different high- and low-relief accommodation/transfer zones (e.g., Tsikalas et al., 2001, 2022) (Figures 3 and 11-inset map). Conversely, the nature of the WRHFC and NURFC invites also to suggest that gravitational processes played an important role on the development of these structural features as some of the faults developed on top of tilted blocks that affect the geometry of the top-basement seismic horizon (Figure 2). Alternatively, dome-like

structures or sedimentary bulges (i.e., South Lofoten margin dome, SLMD; and Northern Vesterålen margin dome, NVMD), and outer highs or volcanic edifices (i.e. Andøya Volcanic Mound, AVM) have been reported in association with the WRHFC and NURFC (e.g., Tsikalas et al., 2022), and further evidence compressional deformation during the Cenozoic (Doré et al., 2008; Gaina et al., 2017) (e.g., Figures 1–3, and 11b). These latter features exist in the present-day studied margins, except where they are eroded by younger late Cenozoic/Quaternary glacial processes (Figures 1, 10 and 11d). Based on all the above we suggest that crustal extension towards breakup may have reactivated the underlying shear zones, and the following readjustments of basement relief, together with different degrees of coupling between the overlying fault complexes may have modified and deformed the sedimentary cover above (Figure 11).

The Late Cretaceous–Palaeocene low-angle detachment faults observed in the upper crust along the WRHFC and NURFC are then suggested to be part of an entire-crust fault system, and in this context, an updated model for lithospheric extension at the conjugate margins is presented in Figure 12. A primary first stage (Figure 12a) is interpreted to be related to a thinning phase during the distinct extensional episodes of the Late Cretaceous–Palaeocene rifting, and this is characterized by low-angle detachment faulting. For instance, the average total extension leading to breakup in the conjugate transect across the Vesterålen segment and the NE Greenland Thetis Basin (central region) is estimated to be ca. 220 km (Figures 10 and 12a), with nearly ca. 48 km corresponding to the combined contribution from the Late Cretaceous–Palaeocene rifting (Abdelmalak et al., 2022). Initially, low-angle faulting at relatively deeper levels is localized to the

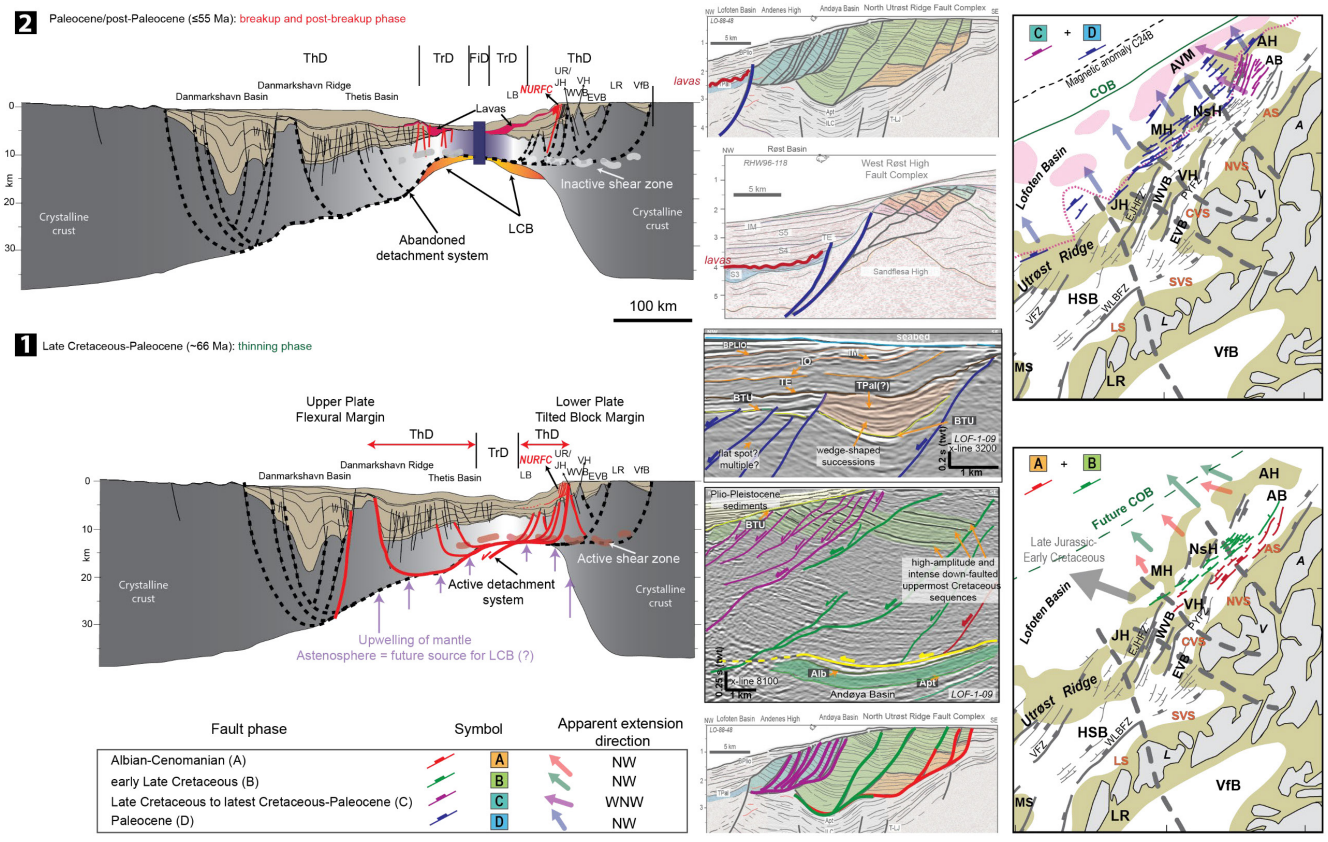

FIGURE 12 Conceptual tectonic model illustrating the multiphase evolution of the Lofoten-Vesterålen (LVM) and NE Greenland conjugate margins (modified from Meza-Cala et al., 2021). The composite Late Cretaceous-Palaeocene rifting and post-Palaeocene tectonic evolution is illustrated following our observations upon the structural analysis of the WRHFC and NURFC fault complexes in the LVM. To the left, the two-step reconstruction of the crustal transect across the listric/detachment system illustrates the extent of the thinning domain (ThD), transitional crust domain (TrD), and the fully igneous domain (FiD). The solid red lines indicate active extensional tectonics, whereas the stippled black lines are the inactive faults of the crustal-scale model that were developed during previous extensional phases. Seismic panels in the centre illustrate the tectono-stratigraphic evolution of the fault complexes with respect to the fault stages. The two map panels to the right show the distribution and extent of fault stages in the central and northern LVM. Coloured fault traces are active, whereas the ones in grey are inactive. Vectors of apparent extension for each fault stage is also schematically indicated in these maps as arrows. Arrow in grey indicates the regional Late Jurassic-Early Cretaceous WNW extension direction.

east of the WRHFC and NURFC fault complexes and corresponds to the early Late Cretaceous fault stages (B and B1-B3), which are interpreted as the initial structuration within the fault complexes. Following that, progressive migration of deformation in time and space was established and is recognized as the Late Cretaceous to latest Cretaceous–Palaeocene fault stages (C and C1-C2) localized towards the west of the fault complexes (Figure 12a). These detachment structures that possibly developed at intermediate-to-deep levels of the continental crust often suggest ductile deformation (e.g., Clerc et al., 2018), and they could have been possibly triggered by thinning mechanisms such as depth-depending stretching as it was proposed for the NE Atlantic margins (e.g., Kusznir et al., 2005) and similar rifted margins worldwide (e.g., Blaich et al., 2011; Deng et al., 2020; Osmundsen & Péron-Pinvidic, 2018; Zhao et al., 2018).

Subsequently, a second stage related to breakup takes place, together with an increase in magmatic activity and abandonment of the suggested detachment system (Figure 12b) (e.g., similar to the Brazilian margin: Blaich et al., 2011). The Palaeocene fault stage (D) is clearly evidenced to represent the westernmost faults on the LVM. It seems these faults become steeper ocean-wards, as some are probably able to reactivate pre-existing structures. Similarly, these faults on both the WRHFC and NURFC fault complexes confine the spatially extensive layer of breakup-related volcano-clastic deposits onto the Lofoten and Røst basins, as well as the few locally observed sedimentary wedges on the upper parts of the NURFC (Figure 12b). Thus, the fault complexes must have been formed prior to the initiation of seafloor spreading, as the breakup lavas cannot flow uphill (e.g., Figure 4 profile 2 and Figure 5 profile 5). Moreover, magmatic processes guided by pre-existing faults and transfer zones (e.g., Figure 3), and/or any other inherited structures may have influenced and governed the final plate separation as they are favoured by the stress directions within the crustal and mantle weakness zones (Schiffer et al., 2020). Similarly, the rheologically-distinct and up-domed lower crustal structures (i.e. LCB) that are formed at the time of rifting and breakup can control the location, deformation and type of breakup, and influence the subsequent basin and crustal development (Figure 12b) (Breivik et al., 2017; Gernigon et al., 2004, 2014; Meza-Cala et al., 2021). The resulting asymmetric rift geometry of the Lofoten-Vesterålen and NE Greenland conjugate margins is presumed to be laterally controlled by listric faults and the configuration of a detachment system through an upper plate or flexural margin (NE Greenland margin), and a lower plate or tilted-block margin (Lofoten-Vesterålen margin) with a suggested subsequent effect on the vertical differentiation across the conjugate system present-day crustal configuration (Figure 12a) (e.g., Mosar et al., 2002).

5.5 | Obliquity of extension towards breakup and margin evolution

The obliquity in the breakup axis location, the extension direction, and areas of focused stretching along the Lofoten-Vesterålen and NE Greenland conjugate margins are constrained mainly from the detailed mapping of fault stages within the NURFC and its vicinity on the central and northern LVM (Figure 12). The corresponding faulting into the southern LVM and within the WRHFC is also expected to be active during the equivalent time periods and towards the outer part of the margin (Figures 2 and 4) (Tsikalas et al., 2019). During most of the mid- and early Late Cretaceous, the deformation (fault stage A) is observed to concentrate mostly towards the central/northern Vesterålen and Andøya margin segments (Figures 8a,b and 12), as the main WNW-ESE directed Late Jurassic-Early Cretaceous extension and regional basin structuring along the LVM is ceased (e.g., Faleide et al., 2008). The Havbåen Sub-basin area up to the NNW–SSE trending Jennegga Transfer Zone is, however, observed with active sedimentation still in Albian times within the northern Lofoten segment (e.g., Meza-Cala et al., 2021; Tsikalas et al., 2001). Locally on the northern LVM, some few NE–SW trending faults are observed to gradually shift into a more NNE–SSW orientation (fault stages B and B1–B3) in the early Late Cretaceous (Figure 12). As deformation moves towards the northwest within the margin, faults eventually became oriented nearly N-S on the Andøya segment during the latest Cretaceous, and thus with a WNW-ESE apparent extension direction (fault stages C and C1–C2; Figure 12). In comparison, a shift in apparent extension direction from WNW to NW has been documented regionally to occur prior to the Campanian (90–83 Ma) (i.e. Hansen et al., 2012), yet the WRHFC and NURFC fault complexes provide better constrained location of the focused area that is being actively deformed, as well as better control on the apparent extension direction with respect to the line of final continental separation towards the end of the Campanian (Figure 12). Similarly, on both the northern Vøring/southern Lofoten-Vesterålen and NE Greenland conjugate margins the regional tectonic quiescence at the end of the Albian had a duration until the next major rifting initiated around Campanian to Maastrichtian times (Gernigon et al., 2003; Lundin & Doré, 1997; Skogseid et al., 2000; Tsikalas et al., 2001; Tsikalas, Faleide, et al., 2005). From this time up to breakup in the Palaeocene/Eocene transition the divergence direction was again shifted to a NW-SE oriented apparent extension direction (fault stage D; Figure 12) and perpendicular to the first magnetic seafloor spreading anomaly.

Numerical modelling of lithospheric-scale rifting to breakup showed that a constant extension direction can generate multiphase fault orientations, and therefore local variations in crustal stress field and fault orientation may arise intrinsically during rift maturation and may not require plate motion changes (Brune, 2014). If we consider the main basin-opening phase as the Late Jurassic-Early Cretaceous has occurred constantly in a WNW extension direction during the entire Late Cretaceous–Palaeocene, the resulting final rifted margin is moderately oblique (ca. 30°–45°) with respect to the breakup line (Figure 12). Such evolution of fault patterns can reproduce during the time of breakup the observed orientation for fault stage D, where these latter faults are localized near the COB region and orthogonal to the seafloor spreading direction (Figure 12). However, transtension and segmentation resulting in oblique rifting across south Lofoten has been proposed possibly due to reactivation of Devonian detachments, differential uplift of fault blocks, and/or basement buoyancy effects due to differences in mineral geochemistry (Wilson et al., 2006 and references therein). Moreover, Henstra et al. (2019) showed that in the presence of inherited pre-Mesozoic structural grain (i.e. earlier rift phase with brittle imprint) contrasting styles of fault growth, such as zigzag geometries and splay faults at the tips of reactivated previous fault systems can result in the south Lofoten area within the Ribban and Vestfjorden basins (Figure 1) (Bergh et al., 2007; Meza-Cala et al., 2021; Tasrianto & Escalona, 2015). The latter findings agree with the evolution of fault activity and fault distribution for the mapped fault stages within the fault complexes and their relationship with basement highs mapped in the area (Figures 3, 11 and 12). No prominent basement highs are observed within the Ribban Basin area (e.g., Havbåen Subbasin), whereas more influence of pre-existing structures is expected towards the north of the Lofoten-Vesterålen margin as basement topography is rougher (Figure 3). This would result in fault stage C at NURFC being oblique to the previously formed fault stages A and B and their apparent extension direction (Figure 12).

6 | SUMMARY AND CONCLUSIONS

An integrated dataset of reprocessed 2D and 3D seismic reflection data, potential field data (gravity and magnetics), and updated published crustal transects have been utilized to investigate the Late Cretaceous–Palaeocene continental crustal extension within the Lofoten-Vesterålen margin (LVM) towards lithospheric breakup between this and its conjugate NE Greenland margin at the Palaeocene-Eocene transition. We focus on the study of two low-angle detachment structures named West Røst High Fault Complex (WRHFC) and North Utrøst Ridge Fault Complex (NURFC) located at the southern and central-northern portions of the LVM, respectively. Extension was calculated from the fault-block geometries (i.e., fault heave and displacement) of the two low-angle detachment fault complexes and were compared with the extension measurements derived from the stretching and thinning factors for the whole-crust within the studied portions of the conjugate margins. Moreover, the amount extension from the fault geometries were corrected for sub-seismic resolution faulting.

The WRHFC and NURFC fault complexes evidence multiple episodes of faulting with various degrees of intensity during the composite Late Cretaceous–Palaeocene rifting that culminated in lithospheric breakup. These faulting episodes were mapped as distinct fault stages that can be age-correlated across both fault complexes due to their specific geometries and corresponding deformation, and they extend over an area that has experienced multiphase thinning further back in time than mid-Cretaceous times. The NURFC has locally recorded an Albian-Cenomanian fault stage (A) related to the initial faulting activity, and with a range of maximum extension of ca. 1.1–1.5 km. However, the main and early faulting activity occurred during the early Late Cretaceous, probably throughout the Cenomanian–Turonian to Campanian (fault stages B and B1–B3). The combined maximum extension ranges estimated for fault stages (B1 to B3) at WRHFC and fault stage (B) at NURFC are, respectively, ca. 3.9–4.7 and 2.2–2.8 km. A less intense rifting compared to the preceded one (e.g., smaller in size individual fault-blocks) is observed as westward faulting activity is developed during the Late Cretaceous to latest Cretaceous–Palaeocene fault stages (C and C1–C2). The combined maximum extension ranges for fault stages (C1 and C2) at WRHFC and the contemporary fault stage (C) at NURFC are, respectively, ca. 1.3–2.5 and 2.5–3.1 km. At last, and close to the time (or during?) breakup, the westernmost Palaeocene fault stage (D) is observed with steeper fault plane geometries that impeded the up-flow of breakup-related volcanic deposits into the inner parts of the LVM. The Palaeocene (D) fault stage maximum extension estimates are in the order of ca. 1.5–2 km at WRHFC and ca. 2–2.6 km at NURFC. Despite the differences in absolute values, the narrower in extent WRHFC has accommodated a relatively greater amount of focused and concentrated extension (ca. 18–19 km), whereas the NURFC has a much wider area with widespread extension intensity (ca. 6–8 km).

The calculated extension at the LVM shows a northwards decreasing trend in magnitude, whereas the magnitude of extension within the conjugate NE Greenland side seems to increase following the same northwards

trend. In addition, extension within the continental crust is observed to increase in magnitude as the presence of lower crustal bodies (LCBs) underplating the crust increases, and as documented in this study (0% and 100% modelled LCB scenarios). Average extension estimates considering 0%–100% LCB scenarios within the southern, central, and northern portions of the LVM are, respectively, ca. 154–170, 63–66, and 40 km. Similarly, average extension estimates considering 0%–100% LCB scenarios within the southern, central, and northern portions of the NE Greenland margin are, respectively, ca. 29–49, 170–171, and 226 km. These estimates when compared to derived extension from seismically observed fault-block geometry suggest an apparent extension discrepancy at the scale of the whole conjugate margin system. Hence, only ca. 11% and 13% of the extension would be seen through the interpreted fault geometries in the studied seismic profiles on the WRHFC and NURFC, respectively. The corrected maximum extension for sub-seismic resolution faulting ranges for both the WRHFC (southern LVM) and NURFC (central and northern LVM) fault complexes are, respectively, ca. 164–173 and 46–62 km.

The Late Cretaceous–Palaeocene WRHFC and NURFC fault complexes provide key evidence for a ductile mode of deformation towards breakup and a multiphase tectonic evolution for the resulting asymmetric rift geometry of the Lofoten-Vesterålen and NE Greenland conjugate margins. The proposed tectonic evolution model includes a primary stage related to thinning phases during early Late Cretaceous (fault stages B and B1–B3) and Late Cretaceous to latest Cretaceous–Palaeocene (fault stages C and C1–C2). Rifting in the conjugate margins is controlled by listric faults and the configuration of a detachment system through an upper plate or flexural margin (NE Greenland margin), and a lower plate or tilted-block margin configuration (LVM). Furthermore, seismic and structural observations on reflection data suggest the existence of a sheared region within the crust, that was possibly active during active stretching before continental separation. The effects of such ductile mode of deformation are manifested as reorganization of basement topography and varying ability to couple deformation within the overlying Cretaceous sedimentary strata consisting mostly of fine-grained lithologies. Subsequently, breakup takes place, together with the development of Palaeocene fault stage (D), an increase in magmatic activity, and abandonment of the suggested detachment system. The obliquity in the breakup axis location along the LVM-NE Greenland conjugate margins can be explained by this model.

ACKNOWLEDGEMENTS

TGS and NPD are acknowledged for providing access to seismic data and permission to publish the examples used in this study. Utilized gravity and magnetic data are courtesy of NGU and Odleiv Olesen. The Petrel software has been used in seismic mapping and Schlumberger is acknowledged for providing academic licences of the software to University of Oslo. Vår Energi is acknowledged for providing the resources to F. Tsikalas to fulfil the study through sponsoring his Adjunct Professor position at University of Oslo. We thank the feedback and comments of Associate Editor Craig Magee and three anonymous reviewers that helped to significantly improve an earlier version of this manuscript.

CONFLICT OF INTEREST STATEMENT

The authors declare that they have no conflict of interest.

PEER REVIEW

The peer review history for this article is available at https://publons.com/publon/10.1111/bre.12756.

DATA AVAILABILITY STATEMENT

The data that support the findings of this study are available from NPD and TGS. Restrictions apply to the availability of these data, which were used under licence for this study.

REFERENCES

Abdelmalak, M. M., Faleide, J. I., Planke, S., Gernigon, L., Zastrozhnov, D., Shephard, G. E., & Myklebust, R. (2017). The T-reflection and the deep crustal structure of the Vøring margin, offshore mid-Norway. *Tectonics*, *36*(11), 2497–2523.

Abdelmalak, M. M., Gac, S., Faleide, J. I., Shephard, G. E., Tsikalas, F., Torsvik, T. H., & Zastrozhnov, D. (2022). Quantification and restoration of the pre-drift extension across the NE Atlantic conjugate margins during the mid-Permian-early Cenozoic multi-rift events. *Tectonics*, *42*, e2022TC007386.

Abdelmalak, M. M., Planke, S., Faleide, J. I., Jerram, D. A., Zastrozhnov, D., Eide, S., & Myklebust, R. (2016). The development of volcanic sequences at rifted margins: New insights from the structure and morphology of the Vøring escarpment, mid-Norwegian margin. *Journal of Geophysical Research: Solid Earth*, *121*, 5212–5236.

Ackermann, R. V., Schlische, R. W., & Withjack, M. O. (2001). The geometric and statistical evolution of normal fault systems: An experimental study of the effects of mechanical layer thickness on scaling laws. *Journal of Structural Geology*, *23*(11), 1803–1819.

Andersen, T. B., & Jamtveit, B. (1990). Uplift of deep crust during orogenic extensional collapse: A model based on field studies in the Sogn-Sunnfjord region of western Norway. *Tectonics*, *9*(5), 1097–1111.

Barnett-Moore, N., Müller, D. R., Williams, S., Skogseid, J., & Seton, M. (2018). A reconstruction of the North Atlantic since the earliest Jurassic. *Basin Research*, *30*, 160–185.

Bergh, S. G., Eig, K., Kløvjan, O. S., Henningsen, T., Olesen, O., & Hansen, J. A. (2007). The Lofoten-Vesterålen continental margin: A multiphase Mesozoic-Palaeogene rifted shelf as shown

by offshore-onshore brittle fault-fracture analysis. *Norwegian Journal of Geology/Norsk Geologisk Forening*, *87*, 29–58.

Berndt, C., Mjelde, R., Planke, S., Shimamura, H., & Faleide, J. I. (2001). Controls on the tectono-magmatic evolution of a volcanic transform margin: The Vøring transform margin, NE-Atlantic. *Marine Geophysical Researches*, *22*(3), 133–152.

Blaich, O. A., Faleide, J. I., & Tsikalas, F. (2011). Crustal breakup and continent-ocean transition at South Atlantic conjugate margins. *Journal of Geophysical Research: Solid Earth*, *116*(B1), e2010JB007686. https://doi.org/10.1029/2010JB007686

Blaich, O. A., Tsikalas, F., & Faleide, J. I. (2017). New insights into the tectono-stratigraphic evolution of the southern Stappen high and its transition to Bjørnøya Basin, SW Barents Sea. *Marine and Petroleum Geology*, *85*, 89–105.

Breivik, A. J., Faleide, J. I., Mjelde, R., & Flueh, E. R. (2009). Magma productivity and early seafloor spreading rate correlation on the northern Vøring margin, Norway—Constraints on mantle melting. *Tectonophysics*, *468*(1–4), 206–223.

Breivik, A. J., Faleide, J. I., Mjelde, R., Flueh, E. R., & Murai, Y. (2017). A new tectono-magmatic model for the Lofoten/Vesterålen margin at the outer limit of the Iceland plume influence. *Tectonophysics*, *718*, 25–44.

Breivik, A. J., Faleide, J. I., Mjelde, R., Flueh, E. R., & Murai, Y. (2020). Crustal structure and erosion of the Lofoten/Vesterålen shelf, northern Norwegian margin. *Tectonophysics*, *776*, 228318.

Breivik, A. J., Mjelde, R., Faleide, J. I., & Murai, Y. (2012). The eastern Jan Mayen microcontinent volcanic margin. *Geophysical Journal International*, *188*, 798–818.

Brekke, H. (2000). *The tectonic evolution of the Norwegian Sea continental margin, with emphasis on the Voring and More basins*. Special Publication-Geological Society of London, *167*, 327–378.

Brueckner, H. K., Gilotti, J. A., & Nutman, A. P. (1998). Caledonian eclogite-facies metamorphism of early Proterozoic protoliths from the north-East Greenland eclogite province. *Contributions to Mineralogy and Petrology*, *130*(2), 103–120.

Brune, S. (2014). Evolution of stress and fault patterns in oblique rift systems: 3-D numerical lithospheric-scale experiments from rift to breakup. *Geochemistry, Geophysics, Geosystems*, *15*(8), 3392–3415.

Claringbould, J. S., Bell, R. E., Jackson, C. A. L., Gawthorpe, R. L., & Odinsen, T. (2017). Pre-existing normal faults have limited control on the rift geometry of the northern North Sea. *Earth and Planetary Science Letters*, *475*, 190–206.

Clerc, C., Ringenbach, J. C., Jolivet, L., & Ballard, J. F. (2018). Rifted margins: Ductile deformation, boudinage, continentward-dipping normal faults and the role of the weak lower crust. *Gondwana Research*, *53*, 20–40.

Corfu, F., & Hartz, E. H. (2011). U–Pb geochronology in Liverpool Land and Canning Land, East Greenland—The complex record of a polyphase Caledonian orogeny. *Canadian Journal of Earth Sciences*, *48*(2), 473–494.

Davis, M., & Kusznir, N. (2004). Depth-dependent lithospheric stretching at rifted continental margins. In *Rheology and deformation of the lithosphere at continental margins* (pp. 92–137). Columbia University Press.

Deng, H., Ren, J., Pang, X., Rey, P. F., McClay, K. R., Watkinson, I. M., Zheng, J., & Luo, P. (2020). South China Sea documents the transition from wide continental rift to continental break up. *Nature Communications*, *11*(1), 1–9.

Dinkelman, M. G., Granath, J. W., & Whittaker, J. M. (2010). The NE Greenland continental margin. *GeoExpro*, *6*, 36–40.

Doré, A. G., Lundin, E. R., Fichler, C., & Olesen, O. (1997). Patterns of basement structure and reactivation along the NE Atlantic margin. *Journal of the Geological Society*, *154*(1), 85–92.

Doré, A. G., Lundin, E. R., Kusznir, N. J., & Pascal, C. (2008). Potential mechanisms for the genesis of Cenozoic domal structures on the NE Atlantic margin: Pros, cons and some new ideas. *Geological Society, London, Special Publications*, *306*(1), 1–26.

Eldholm, O., & Coffin, M. F. (2000). Large igneous provinces and plate tectonics. *Geophysical Monograph-American Geophysical Union*, *121*, 309–326.

Eldholm, O., Gladczenko, T. P., Skogseid, J., & Planke, S. (2000). Atlantic volcanic margins: A comparative study. *Geological Society, London, Special Publications*, *167*(1), 411–428.

Eldholm, O., Tsikalas, F., & Faleide, J. I. (2002). Continental margin off Norway 62–75 N: Palaeogene tectono-magmatic segmentation and sedimentation. *Geological Society, London, Special Publications*, *197*(1), 39–68.

Faleide, J. I., Abdelmalak, M. M., Zastrozhnov, D., Manton, B., Planke, S., & Myklebust, R. (2022). Norwegian Sea Prograded margin Tectono-sedimentary element. In S. S. Drachev, H. Brekke, E. Henriksen, & T. Moore (Eds.), *Sedimentary successions of the Arctic region and their hydrocarbon prospectivity* (p. 57). Geological Society, London, Memoirs.

Faleide, J. I., Bjørlykke, K., & Gabrielsen, R. H. (2015). Geology of the Norwegian continental shelf. In *Petroleum geoscience* (pp. 603–637). Springer.

Faleide, J. I., Pease, V., Curtis, M., Klitzke, P., Minakov, A., Scheck-Wenderoth, M., Kostyuchenko, S., & Zayonchek, A. (2018). *Tectonic implications of the lithospheric structure across the Barents and Kara shelves* (Vol., 460, pp. 285–314). Geological Society, London, Special Publications.

Faleide, J. I., Tsikalas, F., Breivik, A. J., Mjelde, R., Ritzmann, O., Engen, O., Wilson, J., & Eldholm, O. (2008). Structure and evolution of the continental margin off Norway and the Barents Sea. *Episodes*, *31*, 82–91.

Faleide, J. I., Wong, P. W., Hassaan, M., Abdelmalak, M. M., Tsikalas, F., & Gabrielsen, R. H. (2022). West Barents sheared margin composite Tectono-sedimentary element. In S. S. Drachev, H. Brekke, E. Henriksen, & T. Moore (Eds.), *Sedimentary successions of the Arctic region and their hydrocarbon prospectivity* (p. 57). Geological Society, London, Memoirs.

Faleide, J. I., Zastrozhnov, D., Abdelmalak, M. M., Manton, B., Planke, S., Gernigon, L., Brekke, H., & Myklebust, R. (2022). Møre-Vøring composite Tectono-sedimentary element, Norwegian rifted margin, Norwegian Sea. In S. S. Drachev, H. Brekke, E. Henriksen, & T. Moore (Eds.), *Sedimentary successions of the Arctic region and their hydrocarbon prospectivity* (p. 57). Geological Society, London, Memoirs.

Fossen, H. (2010). *Structural geology*. Cambridge University Press.

Fyhn, M. B. W., Hopper, J. R., Sandrin, A., Lauridsen, B. W., Heincke, B. H., Nøhr-Hansen, H., Andersen, M. S., Alsen, P., & Nielsen, T. (2021). Three-phased latest Jurassic–Eocene rifting and mild mid-Cenozoic compression offshore NE Greenland. *Tectonophysics*, *815*, 228990.

Gaina, C., Blischke, A., Geissler, W. H., Kimbell, G. S., & Erlendsson, Ö. (2017). Seamounts and oceanic igneous features in the NE

Atlantic: A link between plate motions and mantle dynamics. *Geological Society, London, Special Publications*, *447*(1), 419–442.

Gernigon, L., Brönner, M., Roberts, D., Olesen, O., Nasuti, A., & Yamasaki, T. (2014). Crustal and basin evolution of the southwestern Barents Sea: From Caledonian orogeny to continental breakup. *Tectonics*, *33*(4), 347–373.

Gernigon, L., Franke, D., Geoffroy, L., Schiffer, C., Foulger, G. R., & Stoker, M. (2020). Crustal fragmentation, magmatism, and the diachronous opening of the Norwegian-Greenland Sea. *Earth-Science Reviews*, *206*, 102839.

Gernigon, L., Ringenbach, J. C., Planke, S., Jonquet-Kolstø, E., Ballard, J. F., & Le Gall, B. (2001). *Rifting and segmentation along the outer Vøring Basin, North Atlantic margin, Norway*. American Association of Petroleum Geologists Annual Meeting.

Gernigon, L., Ringenbach, J. C., Planke, S., & Le Gall, B. (2004). Deep structures and breakup along volcanic rifted margins: Insights from integrated studies along the outer Vøring Basin (Norway). *Marine and Petroleum Geology*, *21*(3), 363–372.

Gernigon, L., Ringenbach, J. C., Planke, S., Le Gall, B., & Jonquet-Kolstø, H. (2003). Extension, crustal structure and magmatism at the outer Vøring Basin, Norwegian margin. *Journal of the Geological Society*, *160*(2), 197–208.

Gernigon, L., Zastrozhnov, D., Planke, S., Manton, B., Abdelmalak, M. M., Olesen, O., Maharjan, D., Faleide, J. I., & Myklebust, R. (2021). A digital compilation of structural and magmatic elements of the mid-Norwegian continental margin (version 1.0). *Norwegian Journal of Geology*, *101*(1), 202112.

Gómez-Romeu, J., Kusznir, N., Roberts, A., & Manatschal, G. (2020). Measurements of the extension required for crustal breakup on the magma-poor Iberia-Newfoundland conjugate margins. *Marine and Petroleum Geology*, *118*, 104403.

Gradstein, F. M., Ogg, J. G., Schmitz, M., & Ogg, G. (2012). *The geologic time scale 2012*. Elsevier.

Hamann, N. E., Wittaker, R. C., & Stemmerik, L. (2005). Geological development of the Northeast Greenland Shelf. In: A.G. Doré, & B.A. Vining (Eds.), *Petroleum Geology: North-West Europe and Global Perspectives-Proceed ings of the 6th Petroleum Geology Conference* (pp. 887–902). Geological Society.

Hansen, J. A., Bergh, S. G., & Henningsen, T. (2012). Mesozoic rifting and basin evolution on the Lofoten and Vesterålen margin, North-Norway; time constraints and regional implications. *Norwegian Journal of Geology/Norsk Geologisk Forening*, *91*(4), 203–228.

Henstra, G. A., Kristensen, T. B., Rotevatn, A., & Gawthorpe, R. L. (2019). How do pre-existing normal faults influence rift geometry? A comparison of adjacent basins with contrasting underlying structure on the Lofoten margin, Norway. *Basin Research*, *31*(6), 1083–1097.

Jakobsson, M., Cherkis, N. Z., Woodward, J., Macnab, R., & Coakley, B. (2000). New grid of Arctic bathymetry aids scientists and mapmakers. *EOS, Transactions American Geophysical Union*, *81*, 89–96.

Koehl, J. B. P., Bergh, S. G., Henningsen, T., & Faleide, J. I. (2018). Middle to late Devonian–carboniferous collapse basins on the Finnmark platform and in the southwesternmost Nordkapp basin, SW Barents Sea. *Solid Earth*, *9*(2), 341–372.

Kusznir, N. J., Hunsdale, R., & Roberts, A. M. (2005). Timing and magnitude of depth-dependent lithosphere stretching on the southern Lofoten and northern Vøring continental margins offshore mid-Norway: Implications for subsidence and hydrocarbon maturation at volcanic rifted margins. In *Geological Society, London, petroleum geology conference series* (Vol. *6*, pp. 767–783). Geological Society of London.

Kusznir, N. J., & Karner, G. D. (2007). Continental lithospheric thinning and breakup in response to upwelling divergent mantle flow: Application to the woodlark, Newfoundland and Iberia margins. In G. D. Karner, G. Manatschal, & L. M. Pinheiro (Eds.), *Imaging, mapping and modelling continental lithosphere extension and breakup* (Vol. *282*, pp. 389–419). Geological Society, London, Special Publications.

Lundin, E. R., & Doré, A. G. (1997). A tectonic model for the Norwegian passive margin with implications for the NE Atlantic: Early cretaceous to break-up. *Journal of the Geological Society*, *154*(3), 545–550.

Manatschal, G., Froitzheim, N., Rubenach, M., & Turrin, B. D. (2001). The role of detachment faulting in the formation of an ocean–continent transition: Insights from the Iberia abyssal plain. In R. C. L. Wilson, R. B. Whitmarsh, B. Taylor, & N. Froitzheim (Eds.), *Non-volcanic rifting of continental margins: Evidence from land and sea* (Vol. *187*, pp. 405–428). Geological Society, London, Special Publications.

Marrett, R., & Allmendinger, R. W. (1992). Amount of extension on "small" faults: An example from the Viking graben. *Geology*, *20*(1), 47–50.

Maystrenko, Y. P., Olesen, O., Gernigon, L., & Gradmann, S. (2017). Deep structure of the Lofoten-Vesterålen segment of the mid-Norwegian continental margin and adjacent areas derived from 3-D density modeling. *Journal of Geophysical Research: Solid Earth*, *122*(2), 1402–1433.

McDermott, K., & Reston, T. (2015). To see, or not to see? *Rifted Margin Extension. Geology*, *43*(11), 967–970.

Meza-Cala, J. C., Tsikalas, F., Faleide, J. I., & Abdelmalak, M. M. (2021). New insights into the late Mesozoic-Cenozoic tectonostratigraphic evolution of the northern Lofoten-Vesterålen margin, offshore Norway. *Marine and Petroleum Geology*, *134*, 105370.

Mjelde, R., Kodaira, S., & Sellevoll, M. A. (1996). Crustal structure of the Lofoten margin, N. Norway, from normal incidence and wide-angle seismic data: A review. *Norwegian Journal of Geology*, *71*, 80.

Mjelde, R., Raum, T., Breivik, A., Shimamura, H., Murai, Y., Takanami, T., & Faleide, J. I. (2005). Crustal structure of the Vøring margin, NE Atlantic: A review of geological implications based on recent OBS data. *Geological Society, London, Petroleum Geology Conference Series*, *6*, 803–813.

Mjelde, R., Raum, T., Murai, Y., & Takanami, T. (2007). Continent–ocean-transitions: Review, and a new tectono-magmatic model of the Vøring plateau, NE Atlantic. *Journal of Geodynamics*, *43*(3), 374–392.

Mjelde, R., & Sellevoll, M. A. (1993). Seismic anisotropy inferred from wide-angle reflections off Lofoten, Norway, indicative of shear-aligned minerals in the upper mantle. *Tectonophysics*, *222*(1), 21–32.

Mohn, G., Karner, G. D., Manatschal, G., & Johnson, C. A. (2015). Structural and stratigraphic evolution of the Iberia–Newfoundland hyper-extended rifted margin: A quantitative modelling approach. *Geological Society, London, Special Publications*, *413*(1), 53–89.

Mosar, J., Eide, E. A., Osmundsen, P. T., Sommaruga, A., & Torsvik, T. H. (2002). Greenland -Norway separation: A geodynamic model for the North Atlantic. *Norwegian Journal of Geology*, *82*, 281–298.

Norlex. (2012). *Standard lithostratigraphy of offshore Norway*. http://nhm2.uio.no/norlex/StandardLithostratigraphicWallchartOffshoreNorway.pdf

Norwegian Petroleum Directorate (NPD). (2010). *Petroleumsressurser i havområdene utenfor Lofoten, Vesterålen og Senja*. http://www.npd.no/Publikasjoner/Rapporter/Petroleumsressurser-i-havomradene-utenfor-Lofoten-Vesteralen-og-Senja---Geofaglig-vurdering/Regional-geologi-og-petroleumsgeologi-Lofoten-Vesteralen-og-Troms-II/

Norwegian Petroleum Directorate (NPD). (2020a). FactPages Norwegian petroleum directorate. https://www.npd.no/en/facts/resource-accounts-and-analysis/resource-accounts-as-of-31-december-2019/

Norwegian Petroleum Directorate (NPD). (2020b). *FactPages Norwegian petroleum directorate*. https://factpages.npd.no/en/wellbore/pageview/exploration/all/2932

Olesen, O., Brönner, M., Ebbing, J., Gellein, J., Gernigon, L., Koziel, J., Lauritsen, T., Myklebust, R., Pascal, C., & Sand, M. (2010). New aeromagnetic and gravity compilations from Norway and adjacent areas: Methods and applications. In *Geological Society, London, Petroleum Geology Conference Series* (Vol. *7*, pp. 559–586). Geological Society of London.

Osmundsen, P. T., & Péron-Pinvidic, G. (2018). Crustal-scale fault interaction at rifted margins and the formation of domain-bounding breakaway complexes: Insights from offshore Norway. *Tectonics*, *37*(3), 935–964.

Phillips, T. B., Magee, C., Jackson, C. A. L., & Bell, R. E. (2018). Determining the three-dimensional geometry of a dike swarm and its impact on later rift geometry using seismic reflection data. *Geology*, *46*(2), 119–122.

Pickering, G., Bull, J. M., & Sanderson, D. J. (1996). Scaling of fault displacements and implications for the estimation of sub-seismic strain. *Geological Society, London, Special Publications*, *99*(1), 11–26.

Ranero, C. R., & Pérez-Gussinyé, M. (2010). Sequential faulting explains the asymmetry and extension discrepancy of conjugate margins. *Nature*, *468*(7321), 294–299.

Ren, S., Skogseid, J., & Eldholm, O. (1998). Late cretaceous-Paleocene extension on the Vøring volcanic margin. *Marine Geophysical Researches*, *20*(4), 343–369.

Reston, T., & McDermott, K. (2014). An assessment of the cause of the 'extension discrepancy' with reference to the West Galicia margin. *Basin Research*, *26*(1), 135–153.

Reston, T. J. (2005). Polyphase faulting during the development of the West Galicia rifted margin. *Earth and Planetary Science Letters*, *237*(3–4), 561–576.

Reston, T. J. (2007). Extension discrepancy at North Atlantic nonvolcanic rifted margins: Depth-dependent stretching or unrecognized faulting? *Geology*, *35*(4), 367–370.

Reston, T. J. (2009). The extension discrepancy and syn-rift subsidence deficit at rifted margins. *Petroleum Geoscience*, *15*(3), 217–237.

Reynolds, P., Planke, S., Millett, J. M., Jerram, D. A., Trulsvik, M., Schofield, N., & Myklebust, R. (2017). Hydrothermal vent complexes offshore Northeast Greenland: A potential role in driving the PETM. *Earth and Planetary Science Letters*, *467*, 72–78.

Rowan, M. G., & Jarvie, A. (2020). Crustal extension and salt tectonics of the Danmarkshavn ridge and adjacent basins, NE Greenland. *Marine and Petroleum Geology*, *117*, 104339.

Schiffer, C., Doré, A. G., Foulger, G. R., Franke, D., Geoffroy, L., Gernigon, L., Holdsworth, B., Kusznir, N., Lundin, E., McCaffrey, K., & Peace, A. L. (2020). Structural inheritance in the North Atlantic. *Earth-Science Reviews*, *206*, 102975.

Skogseid, J. (1994). Dimensions of the late cretaceous-Paleocene Northeast Atlantic rift derived from Cenozoic subsidence. *Tectonophysics*, *240*(1–4), 225–247.

Skogseid, J., Pedersen, T., & Larsen, V. B. (1992). Vøring Basin: Subsidence and tectonic evolution. In *Structural and tectonic modelling and its application to petroleum geology* (pp. 55–82). Elsevier.

Skogseid, J., Planke, S., Faleide, J. I., Pedersen, T., Eldholm, O., & Neverdal, F. (2000). NE Atlantic continental rifting and volcanic margin formation. *Geological Society, London, Special Publications*, *167*(1), 295–326.

Sun, Z., Lin, J., Qiu, N., Jian, Z., Wang, P., Pang, X., Zheng, J., & Zhu, B. (2019). The role of magmatism in the thinning and breakup of the South China Sea continental margin: Special topic: The South China Sea ocean drilling. *National Science Review*, *6*(5), 871–876.

Tasrianto, R., & Escalona, A. (2015). Rift architecture of the Lofoten-Vesterålen margin, offshore Norway. *Marine and Petroleum Geology*, *64*, 1–16.

Tsikalas, F., Eldholm, O., & Faleide, J. I. (2002). Early Eocene Sea floor spreading and continent-ocean boundary between Jan Mayen and Senja fracture zones in the Norwegian-Greenland Sea. *Marine Geophysical Researches*, *23*, 247–270.

Tsikalas, F., Eldholm, O., & Faleide, J. I. (2005). Crustal structure of the Lofoten–Vesterålen continental margin, off Norway. *Tectonophysics*, *404*(3–4), 151–174.

Tsikalas, F., Faleide, J. I., & Eldholm, O. (2001). Lateral variations in tectono-magmatic style along the Lofoten–Vesterålen volcanic margin off Norway. *Marine and Petroleum Geology*, *18*(7), 807–832.

Tsikalas, F., Faleide, J. I., Eldholm, O., & Blaich, O. A. (2012). The NE Atlantic conjugate margins. *Regional Geology and Tectonics: Phanerozoic Passive Margins, Cratonic Basins and Global Tectonic Maps*, *1*, 140–201.

Tsikalas, F., Faleide, J. I., Eldholm, O., & Wilson, J. (2005). Late Mesozoic-Cenozoic structural and stratigraphic correlations between the conjugate mid-Norway and NE Greenland continental margins. In A. G. Doré & B. Vining (Eds.), *Petroleum geology: North-West Europe and global perspectives—Proceedings of the 6th Petroleum Geology Conference* (pp. 785–801). Geological Society, London, Special Publications.

Tsikalas, F., Faleide, J. I., & Kalač, A. (2019). New insights into the cretaceous-Cenozoic tectono-stratigraphic evolution of the southern Lofoten margin, offshore Norway. *Marine and Petroleum Geology*, *110*, 832–855.

Tsikalas, F., Faleide, J. I., & Kusznir, N. J. (2008). Along-strike variations in rifted margin crustal architecture and lithosphere thinning between northern Vøring and Lofoten margin segments off mid-Norway. *Tectonophysics*, *458*(1–4), 68–81.

Tsikalas, F., Meza-Cala, J. C., Abdelmalak, M. M., Faleide, J. I., & Brekke, H. (2022). Lofoten composite Tectono-sedimentary

element, Norwegian rifted margin, Norwegian Sea. *Geological Society, London, Memoirs*, *57*(1), M57-2021.

Voss, M., & Jokat, W. (2007). Continent—Ocean transition and voluminous magmatic underplating derived from P-wave velocity modelling of the East Greenland continental margin. *Geophysical Journal International*, *170*, 580–604.

Voss, M., & Jokat, W. (2009). From Devonian extensional collapse to early Eocene continental break-up: An extended transect of the Kejser Franz Joseph Fjord of the East Greenland margin. *Geophysical Journal International*, *177*(2), 743–754.

Walsh, J., Watterson, J., & Yielding, G. (1991). The importance of small-scale faulting in regional extension. *Nature*, *351*(6325), 391–393.

Wangen, M., Mjelde, R., & Faleide, J. I. (2011). The extension of the Vøring margin (NE Atlantic) in case of different degrees of magmatic underplating. *Basin Research*, *23*(1), 83–100.

White, R. S., Smith, L. K., Roberts, A. W., Christie, P. A. F., Kusznir, N. J., & the rest of the iSIMM Team. (2008). Lower-crustal intrusion on the North Atlantic continental margin. *Nature*, *452*(7186), 460–464.

Wilson, R. W., McCaffrey, K. J., Holdsworth, R. E., Imber, J., Jones, R. R., Welbon, A. I., & Roberts, D. (2006). Complex fault patterns, transtension and structural segmentation of the Lofoten ridge, Norwegian margin: Using digital mapping to link onshore and offshore geology. *Tectonics*, *25*(4), e2005TC001895.

Zastrozhnov, D., Gernigon, L., Gogin, I., Abdelmalak, M. M., Planke, S., Faleide, J. I., Eide, S., & Myklebust, R. (2018). Cretaceous-Paleocene evolution and crustal structure of the northern Vøring margin (offshore mid-Norway): Results from integrated geological and geophysical study. *Tectonics*, *37*(2), 497–528.

Zastrozhnov, D., Gernigon, L., Gogin, I., Planke, S., Abdelmalak, M. M., Polteau, S., Faleide, J. I., Manton, B., & Myklebust, R. (2020). Regional structure and polyphased cretaceous-Paleocene rift and basin development of the mid-Norwegian volcanic passive margin. *Marine and Petroleum Geology*, *115*, 104269.

Zhao, Z., Sun, Z., Liu, J., Pérez-Gussinyé, M., & Zhuo, H. (2018). The continental extension discrepancy and anomalous subsidence pattern in the western Qiongdongnan Basin, South China Sea. *Earth and Planetary Science Letters*, *501*, 180–191.

SUPPORTING INFORMATION

Additional supporting information can be found online in the Supporting Information section at the end of this article.

How to cite this article: Meza-Cala, J. C., Tsikalas, F., Abdelmalak, M. M., & Faleide, J. I. (2023). Structural analysis and measured extension in fault complexes along the Lofoten-Vesterålen margin, offshore Norway, in the context of crustal-scale rifting towards breakup in NE Atlantic. *Basin Research*, *35*, 1329–1361. https://doi.org/10.1111/bre.12756